

Bayesian Uncertainty Estimation for Batch Normalized Deep Networks

Mattias Teye¹ Hossein Azizpour¹ Kevin Smith^{1,2}

Abstract

Deep neural networks have led to a series of breakthroughs, dramatically improving the state-of-the-art in many domains. The techniques driving these advances, however, lack a formal method to account for model uncertainty. While the Bayesian approach to learning provides a solid theoretical framework to handle uncertainty, inference in Bayesian-inspired deep neural networks is difficult. In this paper, we provide a practical approach to Bayesian learning that relies on a regularization technique found in nearly every modern network, *batch normalization*. We show that training a deep network using batch normalization is equivalent to approximate inference in Bayesian models, and we demonstrate how this finding allows us to make useful estimates of the model uncertainty. With our approach, it is possible to make meaningful uncertainty estimates using conventional architectures without modifying the network or the training procedure. Our approach is thoroughly validated in a series of empirical experiments on different tasks and using various measures, outperforming baselines with strong statistical significance and displaying competitive performance with other recent Bayesian approaches.

1. Introduction

Deep learning has dramatically advanced the state of the art in a number of domains, and now surpasses human-level performance for certain tasks such as recognizing the contents of an image (He et al., 2015) and playing Go (Silver et al., 2017). But, despite their unprecedented discriminative power, deep networks are prone to make mistakes. Sometimes, the consequences of mistakes are minor – misidentifying a food dish or a species of flower (Liu et al., 2016) may not be life threatening. But deep networks can already be found in settings where errors carry serious repercussions such as autonomous vehicles (Chen

et al., 2016) and high frequency trading. In medicine, we can soon expect automated systems to screen for skin cancer (Esteva et al., 2017), breast cancer (Shen, 2017), and to diagnose biopsies (Djuric et al., 2017). As autonomous systems based on deep learning are increasingly deployed in settings with the potential to cause physical or economic harm, we need to develop a better understanding of when we can be confident in the estimates produced by deep networks, and when we should be less certain.

Standard deep learning techniques used for supervised learning lack methods to account for uncertainty in the model. The lack of a confidence measure can be especially problematic when the network encounters conditions it was not exposed to during training. Deep networks being susceptible to adversarial examples is an instance of such a problem (Goodfellow et al., 2014), which could cause security hazards due to adversarial attacks. When exposed to data outside of the distribution it was trained on, the network is forced to extrapolate, which can lead to unpredictable behavior. In such cases, if the network can provide information about its uncertainty in addition to its point estimate, disaster may be avoided. This work focuses on estimating such predictive uncertainties in deep networks (Figure 1).

The Bayesian approach provides a theoretical framework for modeling uncertainty (Ghahramani, 2015), which has prompted several attempts to extend neural networks (NN) into a Bayesian setting. Most notably, Bayesian neural networks (BNNs) have been studied since the 1990’s (Neal, 2012), but do not scale well and struggle to compete with modern deep learning architectures. Recently, (Gal & Ghahramani, 2015) developed a practical solution to obtain uncertainty estimates by casting *dropout* training in conventional deep networks as an approximate Bayesian model. They showed that *any network* trained with dropout is an approximate Bayesian model, and uncertainty estimates can be obtained by computing the variance on multiple predictions with different dropout masks.

The inference in this technique, called *Monte Carlo Dropout* (MCDO), has an attractive quality: it can be applied to any pre-trained networks with dropout layer(s). Uncertainty estimates come (nearly) for free. However, in recent years not all architectures use dropout, limiting

¹School of Electrical Engineering and Computer Science, KTH Royal Institute of Technology, Stockholm, Sweden ²Science for Life Laboratory, Solna, Sweden

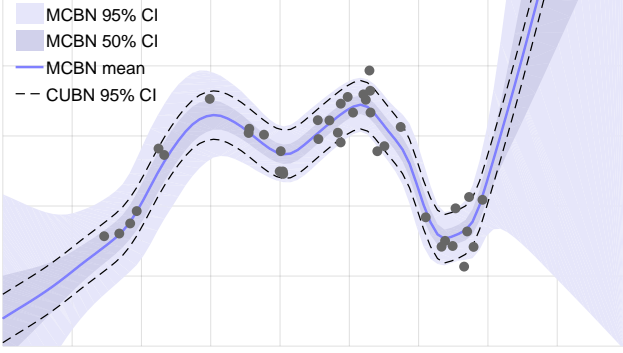


Figure 1. We treat batch-normalized networks (BNN) as approximate Bayesian inference, and thus estimate uncertainty from any pre-trained BNN. For that, several mini-batches are constructed by taking random samples to accompany the query, the mean and variance of the outputs are then considered as the estimation and its uncertainty (MCBN). Here, we show results on a toy dataset from a network with three hidden layers (30 units per layer). Training data is depicted as dots, and the solid line is the predictive mean of 500 stochastic forward passes. Shaded areas represent the model’s uncertainty – the outer area is the 95% CI of the predictive distribution, the inner area is the 50% CI. The dashed lines depicts a minimally useful baseline for uncertainty – the same predictions but with a constant uncertainty chosen to optimize the CRPS uncertainty metric (CUBN). See Section 4.1.

MCDO’s utility. Google’s Inception network, which won ILSVRC in 2014, did not use dropout (Szegedy et al., 2015), nor did the ILSVRC 2015 winner, Microsoft’s residual learning network (He et al., 2016). In place of traditional techniques like dropout, most modern networks have adopted other regularization techniques – *batch normalization* (BN), in particular, has become widespread thanks to its ability to stabilize learning with improved generalization (Ioffe & Szegedy, 2015).

An interesting aspect of BN is that the mini-batch statistics used for training each iteration depend on randomly selected batch members. We exploit this stochasticity and show that training using batch normalization, like dropout, can be cast as an approximate Bayesian inference. We demonstrate how this finding allows us to make meaningful estimates of the model uncertainty in a technique we call *Monte Carlo Batch Normalization* (MCBN) (Figure 1). The method we propose makes no simplifying assumptions on the use of batch normalization, and applies to any network using BN as it appears in practical applications.

We validate our approach by empirical experiments on eight standard datasets used for uncertainty estimation. We measure uncertainty quality relative to a baseline of fixed uncertainty, and show that MCBN outperforms the baseline on nearly all datasets with strong statistical significance. We also show that the uncertainty quality of MCBN is on par with that of MCDO and other recent approximate Bayesian networks. As a practical demonstration,

we apply MCBN to estimate segmentation uncertainty using a conventional segmentation network (Badrinarayanan et al., 2015). Finally, our evaluation makes contributions to help clarify performance of uncertainty estimation models by defining performance bounds on existing metrics and proposing a new visualization that provides an intuitive understanding of uncertainty quality.

2. Related Work

Bayesian models provide a natural framework for modeling uncertainty, and several approaches have been developed to adapt NNs to Bayesian reasoning. A common approach is to place a prior distribution (often a Gaussian) over each parameter. The resulting model corresponds to a Gaussian process for infinite parameters (Neal, 1995), and a Bayesian NN (MacKay, 1992) for a finite number of parameters. Although simple to formulate, inference in BNNs is difficult (Gal, 2016). Focus has thus shifted to techniques to approximate the posterior distribution, leading to *approximate BNNs*. Methods based on variational inference (VI) typically rely on a fully factorized approximate distribution (Kingma & Welling, 2014; Hinton & Van Camp, 1993), but often do not scale. To alleviate these difficulties, (Graves, 2011) proposed a model using sampling methods to estimate a factorized posterior. Another approach, probabilistic backpropagation (PBP), also estimates a factorized posterior via expectation propagation (Hernández-Lobato & Adams, 2015).

Using several strategies to address scaling issues, Deep Gaussian Processes show superior performance in terms of RMSE and uncertainty quality compared to state-of-the-art approximate BNNs (Bui et al., 2016)¹. Another recent approach to Bayesian learning, Bayesian hypernetworks, use a neural network to learn a distribution of parameters over another neural network (Krueger et al., 2017). Multiplicative Normalizing Flows for variational Bayesian networks (MNF) (Louizos & Welling, 2017) is a recent model that formulates a posterior dependent on auxiliary variables. MNF achieves a highly flexible posterior by the application of normalizing flows to the auxiliary variables.

Although these recent techniques address some of the difficulties with approximate BNNs, they all require modifications to the architecture or the way networks are trained, as well as specialized knowledge from practitioners. Recently, (Gal & Ghahramani, 2015) showed that a network trained with dropout implicitly performs the VI objective. Therefore *any* network trained with dropout can be treated as an approximate Bayesian model by making multiple predictions through the network while sampling different

¹By uncertainty quality, we refer to predictive probability distributions as measured by PLL and CRPS.

dropout masks for each prediction. Mean and variance of the predictive distribution can be estimated by the mean and variance of the predictions ².

3. Method

In this work we pose a deep network trained with batch normalization as a *Bayesian model* in order to obtain uncertainty estimates associated with its predictions. In the following, we introduce Bayesian models and a variational approximation using Kullback-Leibler (KL) divergence following (Gal & Ghahramani, 2015). We continue by showing a batch normalized deep network can be seen as an approximate Bayesian model. By employing theoretical insights as well as empirical analysis, we study the induced prior on the parameters when using batch normalization. Finally, we describe the procedure we use for estimating uncertainty of batch normalized deep networks' output.

3.1. Bayesian Modeling

We assume a finite training set $\mathbf{D} = \{(\mathbf{x}_i, \mathbf{y}_i)\}_{i=1:N}$ where each $(\mathbf{x}_i, \mathbf{y}_i)$ is a sample-label pair. Using \mathbf{D} , we are interested in learning an inference function $f_{\omega}(\mathbf{x}, \mathbf{y})$ with parameters ω . In deterministic models, the estimated label $\hat{\mathbf{y}}$ is obtained as follows:

$$\hat{\mathbf{y}} = \arg \max_{\mathbf{y}} f_{\omega}(\mathbf{x}, \mathbf{y})$$

We assume $f_{\omega}(\mathbf{x}, \mathbf{y}) = p(\mathbf{y}|\mathbf{x}, \omega)$ (e.g. in soft-max classifiers), and is normalized to a proper probability distribution. In Bayesian modeling, in contrast to finding a point estimate of the model parameters, the idea is to estimate an (approximate) posterior distribution of the model parameters $p(\omega|\mathbf{D})$ to be used for probabilistic prediction:

$$p(\mathbf{y}|\mathbf{x}, \mathbf{D}) = \int f_{\omega}(\mathbf{x}, \mathbf{y}) p(\omega|\mathbf{D}) d\omega$$

The predicted label, $\hat{\mathbf{y}}$, can then be accordingly obtained by sampling $p(\mathbf{y}|\mathbf{x}, \mathbf{D})$ or taking its maxima.

Variational Approximation In *approximate* Bayesian modeling, a common approach is to learn a parametrized approximating distribution $q_{\theta}(\omega)$ that minimizes $\text{KL}(q_{\theta}(\omega)||p(\omega|\mathbf{D}))$; the Kullback-Leibler (KL) divergence of posterior w.r.t. its approximation, instead of the true posterior. Minimizing this KL divergence is equivalent to the following minimization while being free

²This technique is referred to as “Dropout” in the original work, though we refer to it here as MCDO to avoid confusion with dropout regularization.

of the data term $p(\mathbf{D})$ ³:

$$\begin{aligned} \mathcal{L}_{\text{VA}}(\theta) := & - \sum_{i=1}^N \int q_{\theta}(\omega) \ln f_{\omega}(\mathbf{x}_i, \mathbf{y}_i) d\omega \\ & + \text{KL}(q_{\theta}(\omega)||p(\omega)) \end{aligned}$$

Using Monte Carlo integration to approximate the integral with one realized $\hat{\omega}_i$ for each sample i ⁴, and optimizing over mini-batches of size M , the approximated objective becomes:

$$\hat{\mathcal{L}}_{\text{VA}}(\theta) := - \frac{N}{M} \sum_{i=1}^M \ln f_{\hat{\omega}_i}(\mathbf{x}_i, \mathbf{y}_i) + \text{KL}(q_{\theta}(\omega)||p(\omega)). \quad (1)$$

The first term is the data likelihood and the second term is divergence of the prior w.r.t. the approximated distribution.

3.2. Batch Normalized Deep Nets as Bayesian Modeling

We now describe the optimization procedure of a deep network with batch normalization and draw the resemblance to the approximate Bayesian modeling in Eq (1).

The inference function of a feed-forward deep network with L layers can be described as:

$$f_{\omega}(\mathbf{x}) = \mathbf{W}^L a(\mathbf{W}^{L-1} \dots a(\mathbf{W}^2 a(\mathbf{W}^1 \mathbf{x})))$$

where $a(\cdot)$ is an element-wise nonlinearity function and \mathbf{W}^l is the weight vector at layer l . Furthermore, we denote the input to layer l as \mathbf{x}^l with $\mathbf{x}^1 = \mathbf{x}$ and we then set $\mathbf{h}^l = \mathbf{W}^l \mathbf{x}^l$. Parenthesized super-index for matrices (e.g. $\mathbf{W}^{(j)}$) and vectors (e.g. $x^{(j)}$) indicates j th row and element respectively. Super-index u refers to a specific unit at layer l , (e.g. $\mathbf{W}^u = \mathbf{W}^{l,(j)}, h^u = h^{l,(j)}$). ⁵

Batch Normalization Each layer of a deep network is constructed by several linear units whose parameters are the rows of the weight matrix \mathbf{W} . Batch normalization is a unit-wise operation proposed in (Ioffe & Szegedy, 2015) to standardize the distribution of each unit's input. It essentially converts a unit's output h^u in the following way:

$$\hat{h}^u = \frac{h^u - \mathbb{E}[h^u]}{\sqrt{\text{Var}[h^u]}}$$

³Achieved by constructing the Evidence Lower Bound, called ELBO, and assuming i.i.d. observation noise; details can be found in the Appendix section 1.1.

⁴While a MC integration using a single sample is a weak approximation, in an iterative optimization for θ several samples will be taken over time.

⁵For a (softmax) classification network, $f_{\omega}(\mathbf{x})$ is a vector with $f_{\omega}(\mathbf{x}, \mathbf{y}) = f_{\omega}(\mathbf{x})^{(\mathbf{y})}$, for regression networks with i.i.d. Gaussian noise we have $f_{\omega}(\mathbf{x}, \mathbf{y}) = \mathcal{N}(f_{\omega}(\mathbf{x}), \tau^{-1} \mathbf{I})$.

where the expectations are computed over the training set⁶. Often in deep networks, the weight matrices are optimized using back-propagated errors calculated on mini-batches of data. Therefore, during training, the estimated mean and variance on the mini-batch \mathbf{B} is used, which we denote by $\boldsymbol{\mu}_{\mathbf{B}}$ and $\boldsymbol{\sigma}_{\mathbf{B}}$ respectively. This makes the inference at training time for a sample \mathbf{x} a stochastic process, varying based on other samples in the mini-batch.

Loss Function and Optimization Training deep networks with mini-batch optimization involves a (regularized) risk minimization with the following form:

$$\mathcal{L}_{\text{RR}}(\boldsymbol{\omega}) := \frac{1}{M} \sum_{i=1}^M l(\hat{\mathbf{y}}_i, \mathbf{y}_i) + \Omega(\boldsymbol{\omega})$$

Where the first term is the empirical loss on the training data and the second term is a regularization penalty acting as a prior on model parameters $\boldsymbol{\omega}$. If the loss l is cross-entropy for classification or sum-of-squares for regression problems (assuming i.i.d. Gaussian noise on labels), the first term is equivalent to minimizing the negative log-likelihood:

$$\mathcal{L}_{\text{RR}}(\boldsymbol{\omega}) := -\frac{1}{M\tau} \sum_{i=1}^M \ln f_{\boldsymbol{\omega}}(\mathbf{x}_i, \mathbf{y}_i) + \Omega(\boldsymbol{\omega})$$

with $\tau = 1$ for classification. In a batch normalized network the model parameters are $\{\mathbf{W}^{1:L}, \boldsymbol{\gamma}^{1:L}, \boldsymbol{\beta}^{1:L}, \boldsymbol{\mu}_{\mathbf{B}}^{1:L}, \boldsymbol{\sigma}_{\mathbf{B}}^{1:L}\}$. If we decouple the learnable parameters $\boldsymbol{\theta} = \{\mathbf{W}^{1:L}, \boldsymbol{\gamma}^{1:L}, \boldsymbol{\beta}^{1:L}\}$ from the stochastic parameters $\boldsymbol{\omega} = \{\boldsymbol{\mu}_{\mathbf{B}}^{1:L}, \boldsymbol{\sigma}_{\mathbf{B}}^{1:L}\}$, we get the following objective at each step of the mini-batch optimization of a batch normalized network:

$$\mathcal{L}_{\text{RR}}(\boldsymbol{\theta}) := -\frac{1}{M\tau} \sum_{i=1}^M \ln f_{\{\boldsymbol{\theta}, \hat{\boldsymbol{\omega}}_i\}}(\mathbf{x}_i, \mathbf{y}_i) + \Omega(\boldsymbol{\theta}) \quad (2)$$

where $\hat{\boldsymbol{\omega}}_i$ is the mean and variances for sample i 's mini-batch at a certain training step. Note that while $\hat{\boldsymbol{\omega}}_i$ formally needs to be i.i.d. for each training example, a batch normalized network samples the stochastic parameters once per training step (mini-batch). For a large number of epochs, however, the distribution of sampled batch members for a given training example converges to the i.i.d. case.

Comparing Eq. (1) and Eq. (2) reveals that the optimization objectives are identical if there exists a prior $p(\boldsymbol{\omega})$ corresponding to $\Omega(\boldsymbol{\theta})$ such that $\frac{\partial}{\partial \boldsymbol{\theta}} \text{KL}(q_{\boldsymbol{\theta}}(\boldsymbol{\omega}) || p(\boldsymbol{\omega})) = N\tau \frac{\partial}{\partial \boldsymbol{\theta}} \Omega(\boldsymbol{\theta})$. In a batch normalized network, $q_{\boldsymbol{\theta}}(\boldsymbol{\omega})$ corresponds to the joint distribution of the normalization parameters $\boldsymbol{\mu}_{\mathbf{B}}^{1:L}, \boldsymbol{\sigma}_{\mathbf{B}}^{1:L}$, as implied by the repeated sampling

⁶It also learns an affine transformation for each unit with parameters $\boldsymbol{\gamma}$ and $\boldsymbol{\beta}$, omitted for brevity: $\hat{x}_{\text{affine}}^{(j)} = \boldsymbol{\gamma}^{(j)} \hat{x}^{(j)} + \boldsymbol{\beta}^{(j)}$.

from \mathbf{D} during training. This is an approximation of the true posterior, where we have restricted the posterior to lie within the domain of our parametric network and source of randomness. With that, *we can estimate the uncertainty of predictions from a trained batch normalized network using the inherent stochasticity of BN* (Section 3.4). But first, we discuss the Bayesian prior induced in a typical batch normalized network.

3.3. Prior $p(\boldsymbol{\omega})$

The purpose of $\Omega(\boldsymbol{\theta})$ is to reduce variance in deep networks. L2-regularization, also referred to as weight decay ($\Omega(\boldsymbol{\theta}) = \lambda \sum_{l=1:L} ||W^l||^2$), is a popular technique in deep learning. The induced prior from L2-regularization is studied in the Appendix section 1.5. Under some approximations we find that BN for a deep network with FC layers and ReLU activations induce Gaussian distributions over BN unit's means and standard deviations, centered around the population values given by \mathbf{D} (details in the Appendix, see Eq. 4). Factorizing this distribution across all stochastic parameters and assuming Gaussian priors, we find the approximate corresponding priors:

$$\begin{aligned} p(\boldsymbol{\mu}_{\mathbf{B}}^u) &= \mathcal{N}(0, \frac{J_{l-1}x^2}{2N\tau\lambda_l}) \\ p(\boldsymbol{\sigma}_{\mathbf{B}}^u) &= \mathcal{N}(\mu_p, \sigma_p^2) \end{aligned}$$

where J_{l-1} is the dimensionality of the layer's inputs and x is the average input over \mathbf{D} for all input units. In the absence of scale and shift transformations from the previous BN layer, it converges towards an exact prior for large training datasets and deep networks (under the assumptions of the factorized distribution). The mean and variance for the BN unit's standard deviation, μ_p and σ_p^2 , have no relevance for the reconciliation of the optimization objectives of Eq. (1) and (2).

3.4. Predictive Uncertainty in Batch Normalized Deep Nets

In the absence of the true posterior, we rely on the approximate posterior to express an approximate predictive distribution:

$$p^*(\mathbf{y}|\mathbf{x}, \mathbf{D}) := \int f_{\boldsymbol{\omega}}(\mathbf{x}, \mathbf{y}) q_{\boldsymbol{\theta}}(\boldsymbol{\omega}) d\boldsymbol{\omega}$$

Following (Gal & Ghahramani, 2015) we estimate the first and second moment of the predictive distribution empirically (see Appendix Section 1.4 for details). For regression,

Algorithm 1 MCBN Algorithm

Input: sample x , number of inferences T , batchsize b
Output: mean prediction \hat{y} , predictive uncertainty σ^2

- 1: $\mathbf{y} = \{\}$
- 2: **loop** for T iterations
- 3: $B = \{\}$ \ mini batch
- 4: **loop** for b iterations
- 5: randomly draw $\tilde{x} \in \mathbf{D}$
- 6: $B = B \cup \tilde{x}$
- 7: **end loop**
- 8: $\hat{\omega} = \{\mu_B, \sigma_B\}$ \ mini batch mean and variance
- 9: $\mathbf{y} = \mathbf{y} \cup f_{\hat{\omega}}(x)$
- 10: **end loop**
- 11: $\hat{y} = \mathbb{E}[\mathbf{y}]$
- 12: $\sigma^2 = \text{Cov}[\mathbf{y}] + \tau^{-1}\mathbf{I}$

we have:

$$\mathbb{E}_{p^*}[\mathbf{y}] \approx \frac{1}{T} \sum_{i=1}^T f_{\hat{\omega}_i}(\mathbf{x})$$

$$\text{Cov}_{p^*}[\mathbf{y}] \approx \tau^{-1}\mathbf{I} + \frac{1}{T} \sum_{i=1}^T f_{\hat{\omega}_i}(\mathbf{x})^\top f_{\hat{\omega}_i}(\mathbf{x}) - \mathbb{E}_{p^*}[\mathbf{y}]^\top \mathbb{E}_{p^*}[\mathbf{y}]$$

where each $\hat{\omega}_i$ corresponds to sampling the net's stochastic parameters $\omega = \{\mu_B^{1:L}, \sigma_B^{1:L}\}$ the same way as during training. Sampling $\hat{\omega}_i$ therefore involves sampling a batch \mathbf{B} from the *training set* and updating the parameters in the BN units, just as if we were taking a training step with \mathbf{B} . From a VA perspective, training the network amounted to minimizing $\text{KL}(q_\theta(\omega) || p(\omega|\mathbf{D}))$ wrt θ . Sampling $\hat{\omega}_i$ from the training set, and keeping the size of \mathbf{B} consistent with the mini-batch size used during training, ensures that $q_\theta(\omega)$ during inference remains identical to the approximate posterior optimized during training.

The network is trained just as a regular BN network, the difference is in using the trained network for prediction. Instead of replacing $\omega = \{\mu_B^{1:L}, \sigma_B^{1:L}\}$ with population values from \mathbf{D} , we update these parameters stochastically, once for each forward pass.⁷ Pseudocode for estimating predictive mean and variance is given in Algorithm 1. In our experiments we optimized τ on CRPS using validation data.

4. Experiments and Results

We assess the uncertainty quality of MCBN quantitatively and qualitatively. Our quantitative analysis relies on eight

⁷As an alternative to using the training set \mathbf{D} to sample $\hat{\omega}_i$, we could sample from the implied $q_\theta(\omega)$ as modeled in the Appendix. This would alleviate having to store \mathbf{D} for use during prediction. In our experiments we used \mathbf{D} to sample $\hat{\omega}_i$ however, and leave the evaluation of the modeled $q_\theta(\omega)$ for future research.

Table 1. Properties of the eight regression datasets used to evaluate MCBN. N is the dataset size and Q is the n.o. input features. Only one target feature was used – we used heating load for the Energy Efficiency dataset, which contains multiple target features.

Dataset name	N	Q
Boston Housing	506	13
Concrete Compressive Strength	1,030	8
Energy Efficiency	768	8
Kinematics 8nm	8,192	8
Power Plant	9,568	4
Protein Tertiary Structure	45,730	9
Wine Quality (Red)	1,599	11
Yacht Hydrodynamics	308	6

standard regression datasets, listed in Table 1. Publicly available from the UCI Machine Learning Repository (University of California, 2017) and Delve (Ghahramani, 1996), these datasets have been used to benchmark comparative models in recent related literature (see (Hernández-Lobato & Adams, 2015), (Gal & Ghahramani, 2015), (Bui et al., 2016) and (Li & Gal, 2017)). We report results using standard metrics, and also propose useful upper and lower bounds to normalize these metrics for an easier interpretation in Section 4.2.

Our qualitative results consist of three parts. First, in Figure 1 we demonstrate that MCBN produces reasonable uncertainty bounds on a toy dataset in the style of (Karpathy, 2015). Second, we develop a new visualization of uncertainty quality by plotting test errors sorted by predicted variance in Figure 2. Finally, we apply MCBN to SegNet (Kendall et al., 2015), demonstrating the benefits of MCBN in an existing batch normalized network.

4.1. Metrics

We evaluate uncertainty quality based on two metrics, described below: Predictive Log Likelihood (PLL) and Continuous Ranked Probability Score (CRPS). We also propose upper and lower bounds for these metrics which can be used to normalize them and provide a more meaningful interpretation.

Predictive Log Likelihood (PLL) Predictive Log Likelihood is a widely accepted metric as the main uncertainty quality metric for regression (e.g. (Hernández-Lobato & Adams, 2015), (Gal & Ghahramani, 2015), (Bui et al., 2016) and (Li & Gal, 2017)). A key property is that PLL makes no assumptions about the form of the distribution. The measure is defined for a probabilistic model $f_\omega(\mathbf{x})$ and a single observation $(\mathbf{y}_i, \mathbf{x}_i)$ as:

$$\text{PLL}(f_\omega(\mathbf{x}), (\mathbf{y}_i, \mathbf{x}_i)) = \log p(\mathbf{y}_i | f_\omega(\mathbf{x}_i))$$

where $p(\mathbf{y}_i|f_{\omega}(\mathbf{x}_i))$ is the model’s predicted PDF evaluated at \mathbf{y}_i , given the input \mathbf{x}_i . A more detailed description is given in the Appendix section 1.4. The metric is unbounded and maximized by a perfect prediction (mode at \mathbf{y}_i) with no variance. As the predictive mode moves away from \mathbf{y}_i , increasing the variance tends to increase PLL (by maximizing probability mass at \mathbf{y}_i). While PLL is an elegant measure, it has been criticized for allowing outliers to have an overly negative effect on the score (Selten, 1998).

Continuous Ranked Probability Score (CRPS) Continuous Ranked Probability Score is a measure that takes the full predicted PDF into account with less sensitivity to outliers. A prediction with low variance that is slightly offset from the true observation will receive a higher score from CRPS than PLL. In order for CRPS to be analytically tractable, we need to assume a Gaussian unimodal predictive distribution. CRPS is defined as

$$\text{CRPS}(f_{\omega}(\mathbf{x}_i), (\mathbf{y}_i, \mathbf{x}_i)) = \int_{-\infty}^{\infty} (F(y) - \mathbb{1}(y \geq \mathbf{y}_i))^2 dy$$

where $F(y)$ is the predictive CDF, and $\mathbb{1}(y \geq \mathbf{y}_i) = 1$ if $y \geq \mathbf{y}_i$ and 0 otherwise (for univariate distributions) (Gneiting & Raftery, 2007). CRPS is interpreted as the sum of the squared area between the CDF and 0 where $y < \mathbf{y}_i$ and between the CDF and 1 where $y \geq \mathbf{y}_i$. A perfect prediction with no variance yields a CRPS of 0; for all other cases the value is larger. CRPS has no upper bound.

4.2. Benchmark models and normalized metrics

To establish a lower bound on useful performance for uncertainty estimates, we define a baseline that predicts constant variance regardless of input. The variance is set to a fixed value that optimizes CRPS on validation data. We call this model Constant Uncertainty BN (CUBN). It reflects our best guess of constant variance on test data – thus, any improvement in uncertainty quality from MCBN would indicate a sensible estimate of uncertainty. This benchmark produces identical point estimates as MCBN, which yield the same predictive means. We similarly define a baseline for dropout, Constant Uncertainty Dropout (CUDO). Differences in variance modeling between MCBN, CUBN, MCDO and CUDO are visualized in plots of uncertainty bounds on toy data in Figure 1.

An upper bound on uncertainty performance can also be defined for a probabilistic model f with respect to CRPS or PLL. For each observation $(\mathbf{y}_i, \mathbf{x}_i)$, a value for the predictive variance T_i can be chosen that maximizes PLL or minimizes CRPS⁸. Using CUBN as a lower bound and the optimized CRPS score as the up-

⁸ T_i can be found analytically for PLL, but must be found numerically for CRPS.

per bound, uncertainty estimates can be normalized between these bounds (1 indicating optimal performance, and 0 indicating performance same as fixed uncertainty). We call this normalized measure $\overline{\text{CRPS}} = \frac{\text{CRPS}(f, (\mathbf{y}_i, \mathbf{x}_i)) - \text{CRPS}(f_{\text{CU}}, (\mathbf{y}_i, \mathbf{x}_i))}{\min_T \text{CRPS}(f, (\mathbf{y}_i, \mathbf{x}_i)) - \text{CRPS}(f_{\text{CU}}, (\mathbf{y}_i, \mathbf{x}_i))} \times 100$, and the PLL analogue $\overline{\text{PLL}} = \frac{\text{PLL}(f, (\mathbf{y}_i, \mathbf{x}_i)) - \text{PLL}(f_{\text{CU}}, (\mathbf{y}_i, \mathbf{x}_i))}{\max_T \text{PLL}(f, (\mathbf{y}_i, \mathbf{x}_i)) - \text{PLL}(f_{\text{CU}}, (\mathbf{y}_i, \mathbf{x}_i))} \times 100$. $\overline{\text{CRPS}}$ (and the analogue, $\overline{\text{PLL}}$) establish meaningful scores to measure the performance of an uncertainty model between the trivial solution (constant uncertainty) and *optimal uncertainty* for each prediction.

4.3. Test setup

Our evaluation compares MCBN to MCDO (Gal & Ghahramani, 2015) and MNF (Louizos & Welling, 2017) using the datasets and metrics described above. Our setup is similar to (Hernández-Lobato & Adams, 2015), which was also followed by (Gal & Ghahramani, 2015). However, our comparison implements a different hyperparameter selection, allows for a larger range of dropout rates, and uses larger networks with two hidden layers.

All our models share a similar architecture: two hidden layers with 50 units each, using ReLU activations, with the exception of Protein Tertiary Structure⁹. Input and output data were normalized during training. Results were averaged over five random splits of 20% test and 80% training and cross-validation (CV) data. For each split, 5-fold CV by grid search with a RMSE minimization objective was used to find training hyperparameters and optimal n.o. epochs, out of a maximum of 2000. For BN-based models, the hyperparameter grid consisted of a weight decay factor ranging from 0.1 to 1^{-15} by a log 10 scale, and a batch size range from 32 to 1024 by a log 2 scale. For DO-based models, the hyperparameter grid consisted of the same weight decay range, and dropout probabilities in $\{0.2, 0.1, 0.05, 0.01, 0.005, 0.001\}$. DO-based models used a batch size of 32 in all evaluations. For MNF¹⁰, the n.o. epochs was optimized, the batch size was set to 100, and evaluation for early stopping was performed after each epoch (compared to every 20th for MCBN, MCDO).

For MCBN and MCDO, the model with optimal training hyperparameters was used to optimize τ numerically. This optimization was made in terms of average CV CRPS for MCBN, CUBN, MCDO, and CUDO respectively, before evaluation on the test data.

All estimates for the predictive distribution were obtained by taking 500 stochastic forward passes through the network, throughout training and testing. The implementation was done with TensorFlow. The Adam optimizer was used

⁹With 100 units per hidden layer.

¹⁰Where we used an adapted version of the authors’ code.

Table 2. Uncertainty quality measured on eight datasets. MCBN, MCDO and MNF are compared over 5 random 80-20 splits of the data with 5 different random seeds each split. We report $\overline{\text{CRPS}}$ and $\overline{\text{PLL}}$, uncertainty metrics CRPS and PLL normalized to a lower bound of constant variance and upper bound that maximizes the metric expressed as a percentage (described in Section 4.2). Higher numbers mean the model is closer to the upper bound. We check if the reported values for $\overline{\text{CRPS}}$ and $\overline{\text{PLL}}$ significantly exceed the lower bound using a one sample t-test (significance level indicated by *'s). See text for further details.

Dataset	$\overline{\text{CRPS}}$			$\overline{\text{PLL}}$		
	MCBN	MCDO	MNF	MCBN	MCDO	MNF
Boston	8.50 ****	3.06 ****	5.88 ****	10.49 ****	5.51 ****	1.76 ns
Concrete	3.91 ****	0.93 *	3.13 ***	-36.36 **	10.92 ****	-2.16 ns
Energy	5.75 ****	1.37 ns	1.10 ns	10.89 ****	-14.28 *	-33.88 ns
Kin8nm	2.85 ****	1.82 ****	0.53 ns	1.68 ***	-0.26 ns	0.42 ns
Power	0.24 ***	-0.44 ****	-0.89 ****	0.33 **	3.52 ****	-0.87 ****
Protein	2.66 ****	0.99 ****	0.57 ****	2.56 ***	6.23 ****	0.52 ****
Wine (Red)	0.26 **	2.00 ****	0.94 ****	0.19 *	2.91 ****	0.83 ****
Yacht	-56.39 ***	21.42 ****	24.92 ****	45.58 ****	-41.54 ns	46.19 ****

to train all networks, with a learning rate of 0.001. All code necessary for reproducing both the quantitative and qualitative results is released in an anonymous GitHub repository (<https://github.com/icml-mcbn/mcbn>).

4.4. Test results

A summary of the results measuring uncertainty quality for MCBN, MCDO and MNF are provided in Table 2. Tests were run over eight datasets using 5 random 80-20 splits of the data with 5 different random seeds each split. We report $\overline{\text{CRPS}}$ and $\overline{\text{PLL}}$, expressed as a percentage, which reflects how close the model is to the upper bound. The upper bounds and lower bounds for each metric are described in Section 4.2. We check to see if the reported values of $\overline{\text{CRPS}}$ and $\overline{\text{PLL}}$ significantly exceed the lower bound models using a one sample t-test, where the significance level is indicated by *'s. Further details from the experiment are provided in the Appendix Section 1.6.

In Figure 2 (*left*), we present a novel visualization of uncertainty quality for regression problems. Data are sorted by estimated uncertainty in the x -axis. Grey dots show the errors in model predictions, and the shaded areas show the model uncertainty. A running mean of the errors appears as a gray line. If uncertainty estimation is working well, a correlation should exist between the mean error (gray line) and uncertainty (shaded area). This indicates that the uncertainty estimation recognizes samples with larger (or smaller) potential for predictive errors.

We applied MCBN to an image segmentation task using Bayesian SegNet with the main CamVid and PASCAL-VOC models in (Kendall et al., 2015). This provides a demonstration of how model uncertainty can be obtained on an existing network with minimal effort – simply by running multiple forward passes with different mini-batch constellations randomly taken from the train set. The pre-trained models were obtained from the online model zoo,

and have BN blocks after each layer. We recalculate mean and variance for the first 2 blocks only and use the training statistics for the rest of the blocks¹¹. Due to the GPU memory limit, mini-batches of size 10 and 36 were used for CamVid and VOC respectively. 20 inferences were conducted to estimate the mean and variance of MCBN. Qualitative visual results appear in Figure 2 (*right*), showing high uncertainty near object boundaries. The VOC results are more appealing because of larger mini-batches. It is possible to obtain quantitative measures for various segmentation datasets, but requires tuning the architecture for a fair comparison, and thus is beyond the scope of our work.

Additional experimental results are provided in the Appendix. In Tables 1 and 2, we show the mean $\overline{\text{CRPS}}$ and $\overline{\text{PLL}}$ values. These results indicate that MCBN performs on par with or better than MCDO and MNF across several datasets. Table 3 provides the raw CRPS and PLL scores. In Table 4 we provide RMSE results of the MCBN and MCDO networks in comparison with non-stochastic BN and DO networks. These results indicate that the procedure of multiple forward passes in MCBN and MCDO show slight improvements in the predictive accuracy of the network. Uncertainty-error plots are provided in the Appendix for all the datasets.

5. Discussion

The results presented in Table 2 and the Appendix Tables 1,2,3 indicate that MCBN generates meaningful uncertainty estimates which correlate with actual errors in the model's prediction. We show statistically significant improvements over CUBN in the majority of the datasets, both in terms of $\overline{\text{CRPS}}$ and $\overline{\text{PLL}}$. The visualizations in Figure 2 and in the Appendix Figures 3,4 show correlations between the estimated model uncertainty and errors

¹¹recalculating all blocks which showed less stable predictions

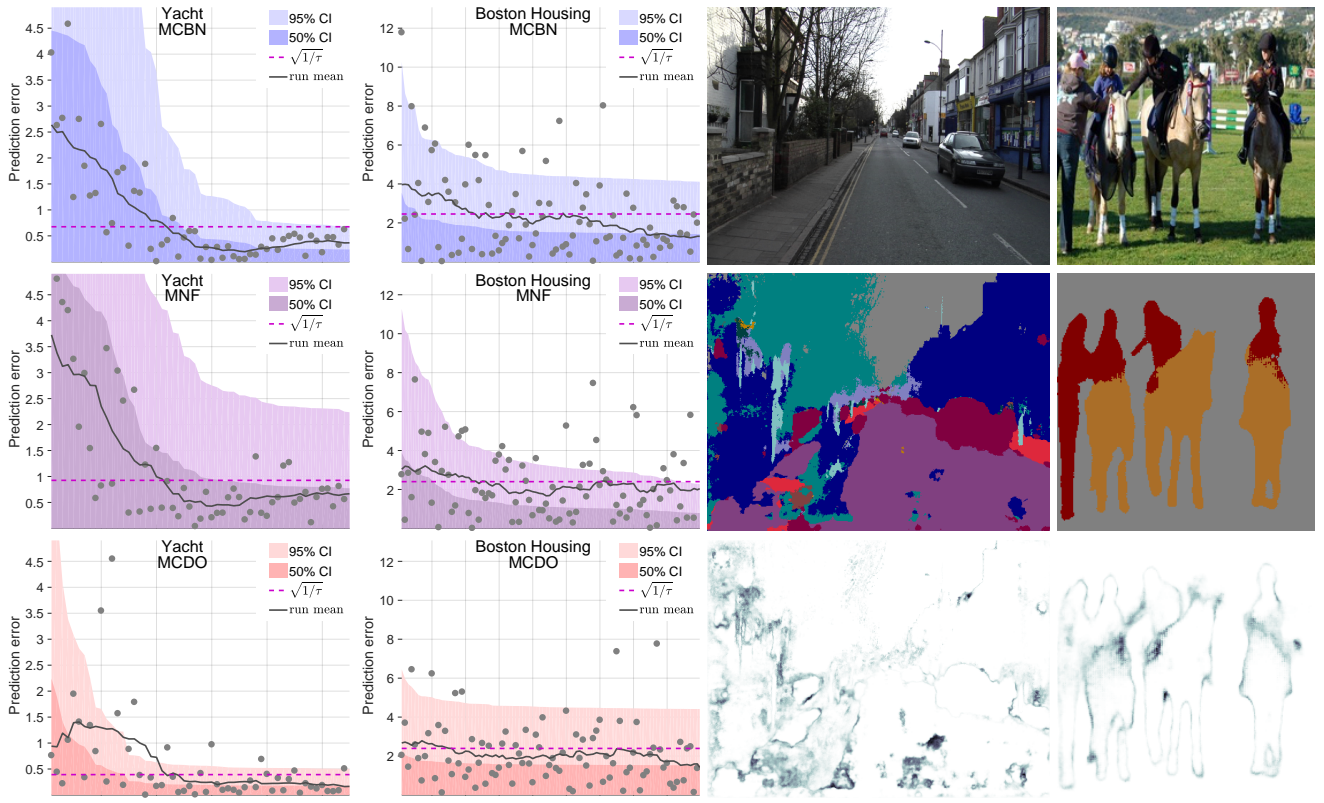


Figure 2. (left) Uncertainty-error plots. Errors in predictions (gray dots) sorted by estimated uncertainty on select datasets. The shaded areas show model uncertainty for MCBN (blue), MNF (violet) and MCDO (red). The light area indicates 95% CI, dark area 50% CI. Gray dots show absolute prediction errors on the test set, and the gray line depicts a running mean of the errors. The dashed line indicates the uncertainty estimates are meaningful for estimating errors. See Appendix for complete results. (right) Results applying MCBN to Bayesian SegNet (Kendall et al., 2015) on scenes from CamVid (left) and PASCAL-VOC (right). Top: original. Middle: the Bayesian estimated segmentation. Bottom: estimated uncertainty using MCBN for all classes. The uncertainty maps for both datasets are reasonable, however, they are qualitatively better for the PASCAL-VOC dataset. This is due to the larger mini-batch size used for PASCAL-VOC (36) compared to CamVid (10). Smaller batchsizes were used for CamVid due to memory limitations (CamVid images are 360x480 while VOC are 224x224).

of the network’s predictions. We perform the same experiments using MCDO and MNF, and find that MCBN generally performs on par with both methods. Looking closer, MCBN outperforms MCDO and MNF in more cases than not, measured by CRPS. However, care must be used with this comparison. The learned network parameters are different, leading to different predictive means which can confound direct comparison.

The results on the Yacht Hydrodynamics dataset seem contradictory. The CRPS score for MCBN are extremely negative, while the PLL score is extremely positive. The opposite trend is observed for MCDO. To add to the puzzle, the visualization in Figure 2 depicts an extremely promising uncertainty estimation that models the predictive errors with high fidelity. We hypothesize that this strange behavior is due to the small size of the data set, which only contains 60 test samples, or due to the Gaussian assumption of CRPS. There is also a large variability in the model’s

accuracy on this dataset, which further confounds the measurements for such limited data.

One might criticize the overall quality of uncertainty estimates observed in all the models we tested, due to the magnitude of CRPS and PLL in Table 2. The scores rarely exceed 10% improvement over the lower bound. However, we caution that these measures should be taken in context. The upper bound is very difficult to achieve in practice – it is optimized for *each test sample individually*. Furthermore, the lower bound is a quite reasonable estimate, it is the optimal fixed value for the entire dataset.

Our approximation of the implied prior in the Appendix provides a new interpretation of the empirical evidence that significantly lower λ should be used in batch normalized networks (Ioffe & Szegedy, 2015). From a VA perspective, too strong a regularization for a given dataset size could be seen as constraining the prior distribution of BN units’ means, effectively narrowing the approximate posterior.

In this work, we have shown that training a deep network using batch normalization is equivalent to approximate inference in Bayesian models. Using our approach, it is possible to make meaningful uncertainty estimates using conventional architectures without modifying the network or the training procedure. We show evidence that the uncertainty estimates from MCBN correlate with actual errors in the model’s prediction, and are useful for practical tasks such as regression or semantic image segmentation. Our experiments show that MCBN yields an improvement over the baseline of optimized constant uncertainty on par with MCDO and MNF. Finally, we make contributions to the evaluation of uncertainty quality by suggesting new evaluation metrics based on useful baselines and upper bounds, and proposing a new visualization which gives an intuitive explanation of uncertainty quality.

Finally, it should be noted that over the past few years, batch normalization has become an integral part of most – if not all – cutting edge deep networks. The potential impact of our work to provide easy access to meaningful uncertainty estimates should not be overlooked.

References

Badrinarayanan, Vijay, Kendall, Alex, and Cipolla, Roberto. Segnet: A deep convolutional encoder-decoder architecture for image segmentation. *arXiv preprint arXiv:1511.00561*, 2015.

Bui, Thang D., Hernández-Lobato, Daniel, Li, Yingzhen, Hernández-Lobato, José Miguel, and Turner, Richard E. Deep Gaussian Processes for Regression using Approximate Expectation Propagation. In *ICML*, 2016.

Chen, Xiaozhi, Kundu, Kaustav, Zhang, Ziyu, Ma, Huimin, Fidler, Sanja, and Urtasun, Raquel. Monocular 3d object detection for autonomous driving. In *Proceedings of the IEEE Conference on Computer Vision and Pattern Recognition*, pp. 2147–2156, 2016.

Djuric, Ugljesa, Zadeh, Gelareh, Aldape, Kenneth, and Diamandis, Phedias. Precision histology: how deep learning is poised to revitalize histomorphology for personalized cancer care. *npj Precision Oncology*, 1(1):22, 2017.

Esteva, Andre, Kuprel, Brett, Novoa, Roberto A., Ko, Justin, Swetter, Susan M., Blau, Helen M., and Thrun, Sebastian. Dermatologist-level classification of skin cancer with deep neural networks. *Nature*, Feb 2017.

Gal, Yarin. *Uncertainty in Deep Learning*. PhD thesis, University of Cambridge, 2016.

Gal, Yarin and Ghahramani, Zoubin. Dropout as a Bayesian Approximation : Representing Model Uncertainty in Deep Learning. *ICML*, 48:1–10, 2015.

Ghahramani, Zoubin. *Delve Datasets*. University of Toronto, 1996. URL <http://www.cs.toronto.edu/~delve/data/kin/desc.html>.

Ghahramani, Zoubin. Probabilistic machine learning and artificial intelligence. *Nature*, 521(7553):452–459, May 2015.

Gneiting, Tilman and Raftery, Adrian E. Strictly Proper Scoring Rules, Prediction, and Estimation. *Journal of the American Statistical Association*, 102(477):359–378, 2007.

Goodfellow, Ian J., Shlens, Jonathon, and Szegedy, Christian. Explaining and harnessing adversarial examples. *arXiv preprint arXiv:1412.6572*, 2014.

Graves, Alex. Practical Variational Inference for Neural Networks. *NIPS*, 2011.

He, Kaiming, Zhang, Xiangyu, Ren, Shaoqing, and Sun, Jian. Delving deep into rectifiers: Surpassing human-level performance on imagenet classification. In *Proceedings of the IEEE international conference on computer vision*, pp. 1026–1034, 2015.

He, Kaiming, Zhang, Xiangyu, Ren, Shaoqing, and Sun, Jian. Deep residual learning for image recognition. In *Proceedings of the IEEE conference on computer vision and pattern recognition*, pp. 770–778, 2016.

Hernández-Lobato, José Miguel and Adams, Ryan. Probabilistic backpropagation for scalable learning of bayesian neural networks. In *International Conference on Machine Learning*, pp. 1861–1869, 2015.

Hinton, Geoffrey E and Van Camp, Drew. Keeping the neural networks simple by minimizing the description length of the weights. In *Proceedings of the sixth annual conference on Computational learning theory*, pp. 5–13. ACM, 1993.

Ioffe, Sergey and Szegedy, Christian. Batch Normalization: Accelerating Deep Network Training by Reducing Internal Covariate Shift. *Arxiv*, 2015. URL <http://arxiv.org/abs/1502.03167>.

Karpathy, Andrej. Convnetjs demo: toy 1d regression, 2015. URL <http://cs.stanford.edu/people/karpathy/convnetjs/demo/regression.html>.

Kendall, Alex, Badrinarayanan, Vijay, and Cipolla, Roberto. Bayesian SegNet: Model Uncertainty in Deep Convolutional Encoder-Decoder Architectures for Scene

Understanding. *CoRR*, abs/1511.0, 2015. URL <http://arxiv.org/abs/1511.02680>.

Kingma, Diederik P and Welling, Max. Auto-Encoding Variational Bayes. In *ICLR*, 2014.

Krueger, David, Huang, Chin-Wei, Islam, Riashat, Turner, Ryan, Lacoste, Alexandre, and Courville, Aaron. Bayesian hypernetworks. *arXiv preprint arXiv:1710.04759*, 2017.

Lehmann, Erich Leo. *Elements of Large-Sample Theory*. Springer Verlag, New York, 1999. ISBN 0387985956.

Li, Yingzhen and Gal, Yarin. Dropout Inference in Bayesian Neural Networks with Alpha-divergences. *arXiv*, 2017.

Liu, Xiao, Xia, Tian, Wang, Jiang, Yang, Yi, Zhou, Feng, and Lin, Yuanqing. Fully convolutional attention networks for fine-grained recognition. *arXiv preprint arXiv:1603.06765*, 2016.

Louizos, Christos and Welling, Max. Multiplicative normalizing flows for variational Bayesian neural networks. In Precup, Doina and Teh, Yee Whye (eds.), *Proceedings of the 34th International Conference on Machine Learning*, volume 70 of *Proceedings of Machine Learning Research*, pp. 2218–2227, International Convention Centre, Sydney, Australia, 06–11 Aug 2017. PMLR. URL <http://proceedings.mlr.press/v70/louizos17a.html>.

MacKay, David JC. A practical bayesian framework for backpropagation networks. *Neural computation*, 4(3):448–472, 1992.

Neal, Radford M. *BAYESIAN LEARNING FOR NEURAL NETWORKS*. PhD thesis, University of Toronto, 1995.

Neal, Radford M. *Bayesian learning for neural networks*, volume 118. Springer Science & Business Media, 2012.

Selten, Reinhard. Axiomatic characterization of the quadratic scoring rule. *Experimental Economics*, 1(1):43–62, 1998.

Shen, Li. End-to-end training for whole image breast cancer diagnosis using an all convolutional design. *arXiv preprint arXiv:1708.09427*, 2017.

Silver, David, Schrittwieser, Julian, Simonyan, Karen, Antonoglou, Ioannis, Huang, Aja, Guez, Arthur, Hubert, Thomas, Baker, Lucas, Lai, Matthew, Bolton, Adrian, Chen, Yutian, Lillicrap, Timothy, Hui, Fan, Sifre, Laurent, van den Driessche, George, Graepel, Thore, and Hassabis, Demis. Mastering the game of go without human knowledge. *Nature*, 550(7676):354–359, Oct 2017.

Szegedy, Christian, Liu, Wei, Jia, Yangqing, Sermanet, Pierre, Reed, Scott, Anguelov, Dragomir, Erhan, Dumitru, Vanhoucke, Vincent, and Rabinovich, Andrew. Going deeper with convolutions. In *Proceedings of the IEEE conference on computer vision and pattern recognition*, pp. 1–9, 2015.

University of California, Irvine. UC Irvine Machine Learning Repository, 2017. URL <https://archive.ics.uci.edu/ml/index.html>.

Wang, Sida I and Manning, Christopher D. Fast dropout training. *Proceedings of the 30th International Conference on Machine Learning*, 28:118–126, 2013. URL <http://machinelearning.wustl.edu/mlpapers/papers/wang13a>.

1. Appendix

1.1. Variational Approximation

Assume we were to come up with a family of distributions parametrised by θ in order to approximate the posterior, $q_\theta(\omega)$. Our goal is to set θ such that $q_\theta(\omega)$ is as similar to $p(\omega|\mathbf{D})$ as possible.

One strategy is to minimize $\text{KL}(q_\theta(\omega)||p(\omega|\mathbf{D}))$, the KL divergence of $p(\omega|\mathbf{D})$ wrt $q_\theta(\omega)$. Minimizing $\text{KL}(q_\theta(\omega)||p(\omega|\mathbf{D}))$ is equivalent to maximizing the ELBO:

$$\int_{\omega} q_\theta(\omega) \ln p(\mathbf{Y}|\mathbf{X}, \omega) d\omega - \text{KL}(q_\theta(\omega)||p(\omega))$$

Assuming i.i.d. observation noise, this is equivalent to minimizing:

$$\mathcal{L}_{\text{VA}}(\theta) := - \sum_{n=1}^N \int_{\omega} q_\theta(\omega) \ln p(\mathbf{y}_i|f_{\omega}(\mathbf{x}_i)) d\omega + \text{KL}(q_\theta(\omega)||p(\omega))$$

Instead of making the optimization on the full training set, we can use a subsampling (yielding an unbiased estimate of $\mathcal{L}_{\text{VA}}(\theta)$) for iterative optimization (as in mini-batch optimization):

$$\hat{\mathcal{L}}_{\text{VA}}(\theta) := - \frac{N}{M} \sum_{i \in B} \int_{\omega} q_\theta(\omega) \ln p(\mathbf{y}_i|f_{\omega}(\mathbf{x}_i)) d\omega + \text{KL}(q_\theta(\omega)||p(\omega))$$

We now make a reparametrisation, due to (Kingma & Welling, 2014): set $\omega = g(\theta, \epsilon)$ where ϵ is a RV. The function g and the distribution of ϵ must be such that $p(g(\theta, \epsilon)) = q_\theta(\omega)$. Assume $q_\theta(\omega)$ can be written $\int_{\epsilon} q_\theta(\omega|\epsilon)p(\epsilon)d\epsilon$ where $q_\theta(\omega|\epsilon) = \delta(\omega - g(\theta, \epsilon))$. Using this reparametrisation we get:

$$\hat{\mathcal{L}}_{\text{VA}}(\theta) = - \frac{N}{M} \sum_{i \in B} \int_{\epsilon} p(\epsilon) \ln p(\mathbf{y}_i|f_{g(\theta, \epsilon)}(\mathbf{x}_i)) d\epsilon + \text{KL}(q_\theta(\omega)||p(\omega))$$

1.2. KL Divergence of factorized Gaussians

If $q_\theta(\omega)$ and $p(\omega)$ factorize over all stochastic parameters:

$$\begin{aligned} \text{KL}(q_\theta(\omega)||p(\omega)) &= - \int_{\omega} \prod_i [q_\theta(\omega_i)] \ln \frac{\prod_i p(\omega_i)}{\prod_i q_\theta(\omega_i)} d\omega \\ &= - \int_{\omega} \prod_i [q_\theta(\omega_i)] \sum_i \left[\ln \frac{p(\omega_i)}{q_\theta(\omega_i)} \right] \prod_i d\omega_i \\ &= \sum_j \left[- \int_{\omega} \prod_i [q_\theta(\omega_i)] \ln \frac{p(\omega_j)}{q_\theta(\omega_j)} \prod_i d\omega_i \right] \\ &= \sum_j \left[- \int_{\omega_j} q_\theta(\omega_j) \ln \frac{p(\omega_j)}{q_\theta(\omega_j)} d\omega_j \int_{\omega_{i \neq j}} \prod_{i \neq j} q_\theta(\omega_i) d\omega_i \right] \\ &= \sum_i - \int_{\omega_i} q_\theta(\omega_i) \ln \frac{p(\omega_i)}{q_\theta(\omega_i)} d\omega_i \\ &= \sum_i \text{KL}(q_\theta(\omega_i)||p(\omega_i)) \end{aligned} \tag{3}$$

such that $\text{KL}(q_{\theta}(\omega) || p(\omega))$ is the sum of the KL divergence terms for the individual stochastic parameters ω_i . If the factorized distributions are Gaussians, where $q_{\theta}(\omega_i) = \mathcal{N}(\mu_q, \sigma_q^2)$ and $p(\omega_i) = \mathcal{N}(\mu_p, \sigma_p^2)$ we get:

$$\begin{aligned}
 \text{KL}(q_{\theta}(\omega_i) || p(\omega_i)) &= \int_{\omega_i} q_{\theta}(\omega_i) \ln \frac{q_{\theta}(\omega_i)}{p(\omega_i)} d\omega_i \\
 &= -H(q_{\theta}(\omega_i)) - \int_{\omega_i} q_{\theta}(\omega_i) \ln p(\omega_i) d\omega_i \\
 &= -\frac{1}{2}(1 + \ln(2\pi\sigma_q^2)) \\
 &\quad - \int_{\omega_i} q_{\theta}(\omega_i) \ln \frac{1}{(2\pi\sigma_p^2)^{1/2}} \exp \left\{ -\frac{(\omega_i - \mu_p)^2}{2\sigma_p^2} \right\} d\omega_i \\
 &= -\frac{1}{2}(1 + \ln(2\pi\sigma_q^2)) \\
 &\quad + \frac{1}{2} \ln(2\pi\sigma_p^2) + \frac{\mathbb{E}_q[\omega_i^2] - 2\mu_p \mathbb{E}_q[\omega_i] + \mu_p^2}{2\sigma_p^2} \\
 &= \ln \frac{\sigma_p}{\sigma_q} + \frac{\sigma_q^2 + (\mu_q - \mu_p)^2}{2\sigma_p^2} - \frac{1}{2}
 \end{aligned} \tag{4}$$

for each KL divergence term. Here $H(q_{\theta}(\omega_i)) = \frac{1}{2}(1 + \ln(2\pi\sigma_q^2))$ is the differential entropy of $q_{\theta}(\omega_i)$.

1.3. Distribution of μ_B^u, σ_B^u

Here we approximate the distribution of mean and standard deviation of a mini-batch, separately to two Gaussians – This has also been empirically verified, see Figure 3 for 2 sample plots and the appendix section 1.8 for more. For the mean we get:

$$\mu_B = \frac{\sum_{m=1}^M \mathbf{W}^{(j)} \mathbf{x}_m}{M}$$

where \mathbf{x}_m are the examples in the sampled batch. We will assume these are sampled i.i.d.¹². Samples of the random variable $\mathbf{W}^{(j)} \mathbf{x}_m$ are then i.i.d.. Then by central limit theorem (CLT) the following holds for sufficiently large M (often ≥ 30):

$$\mu_B \sim \mathcal{N}(\mu, \frac{\sigma^2}{M})$$

For standard deviation:

$$\sigma_B = \sqrt{\frac{\sum_{m=1}^M (\mathbf{W}^{(j)} \mathbf{x}_m - \mu_B)^2}{M}}$$

Then

$$\sqrt{M}(\sigma_B - \sigma) = \sqrt{M} \left(\sqrt{\frac{\sum_{m=1}^M (\mathbf{W}^{(j)} \mathbf{x}_m - \mu_B)^2}{M}} - \sqrt{\sigma^2} \right)$$

We want to rewrite $\sqrt{\frac{\sum_{m=1}^M (\mathbf{W}^{(j)} \mathbf{x}_m - \mu_B)^2}{M}}$. We take a Taylor expansion of $f(x) = \sqrt{x}$ around $a = \sigma^2$. With $x = \frac{\sum_{m=1}^M (\mathbf{W}^{(j)} \mathbf{x}_m - \mu_B)^2}{M}$:

$$\sqrt{x} = \sqrt{\sigma^2} + \frac{1}{2\sqrt{\sigma^2}}(x - \sigma^2) + \mathcal{O}[(x - \sigma^2)^2]$$

¹²Although in practice with deep learning, mini-batches are sampled without replacement, stochastic gradient descent samples with replacement in its standard form.

so

$$\begin{aligned}
 \sqrt{M}(\sigma_B - \sigma) &= \sqrt{M} \left(\frac{1}{2\sqrt{\sigma^2}} \left(\frac{\sum_{m=1}^M (\mathbf{W}^{(j)} \mathbf{x}_m - \mu_B)^2}{M} - \sigma^2 \right) + \right. \\
 &\quad \left. \mathcal{O} \left[\left(\frac{\sum_{m=1}^M (\mathbf{W}^{(j)} \mathbf{x}_m - \mu_B)^2}{M} - \sigma^2 \right)^2 \right] \right) \\
 &= \frac{\sqrt{M}}{2\sigma} \left(\frac{1}{M} \sum_{m=1}^M (\mathbf{W}^{(j)} \mathbf{x}_m - \mu_B)^2 - \sigma^2 \right) + \\
 &\quad \mathcal{O} \left[\sqrt{M} \left(\frac{\sum_{m=1}^M (\mathbf{W}^{(j)} \mathbf{x}_m - \mu_B)^2}{M} - \sigma^2 \right)^2 \right] \\
 &= \frac{1}{2\sigma\sqrt{M}} \left(\sum_{m=1}^M (\mathbf{W}^{(j)} \mathbf{x}_m - \mu_B)^2 - M\sigma^2 \right) + \\
 &\quad \mathcal{O} \left[\sqrt{M} \left(\frac{\sum_{m=1}^M (\mathbf{W}^{(j)} \mathbf{x}_m - \mu_B)^2}{M} - \sigma^2 \right)^2 \right]
 \end{aligned}$$

consider $\sum_{m=1}^M (\mathbf{W}^{(j)} \mathbf{x}_m - \mu_B)^2$. We know that $E[\mathbf{W}^{(j)} \mathbf{x}_m] = \mu$ and write

$$\begin{aligned}
 &\sum_{m=1}^M (\mathbf{W}^{(j)} \mathbf{x}_m - \mu_B)^2 \\
 &= \sum_{m=1}^M ((\mathbf{W}^{(j)} \mathbf{x}_m - \mu) - (\mu_B - \mu))^2 \\
 &= \sum_{m=1}^M ((\mathbf{W}^{(j)} \mathbf{x}_m - \mu)^2 + (\mu_B - \mu)^2 - 2(\mathbf{W}^{(j)} \mathbf{x}_m - \mu)(\mu_B - \mu)) \\
 &= \sum_{m=1}^M (\mathbf{W}^{(j)} \mathbf{x}_m - \mu)^2 + M(\mu_B - \mu)^2 - 2(\mu_B - \mu) \sum_{m=1}^M (\mathbf{W}^{(j)} \mathbf{x}_m - \mu) \\
 &= \sum_{m=1}^M (\mathbf{W}^{(j)} \mathbf{x}_m - \mu)^2 - M(\mu_B - \mu)^2 \\
 &= \sum_{m=1}^M ((\mathbf{W}^{(j)} \mathbf{x}_m - \mu)^2 - (\mu_B - \mu)^2)
 \end{aligned}$$

then

$$\begin{aligned}
 \sqrt{M}(\sigma_B - \sigma) &= \frac{1}{2\sigma\sqrt{M}} \left(\sum_{m=1}^M ((\mathbf{W}^{(j)} \mathbf{x}_m - \mu)^2 - (\mu_B - \mu)^2) - M\sigma^2 \right) + \\
 &\quad \mathcal{O} \left[\sqrt{M} \left(\frac{\sum_{m=1}^M (\mathbf{W}^{(j)} \mathbf{x}_m - \mu_B)^2}{M} - \sigma^2 \right)^2 \right] \\
 &= \frac{1}{2\sigma\sqrt{M}} \left(\sum_{m=1}^M ((\mathbf{W}^{(j)} \mathbf{x}_m - \mu)^2 - \sum_{m=1}^M (\mu_B - \mu)^2 - M\sigma^2) \right) + \\
 &\quad \mathcal{O} \left[\sqrt{M} \left(\frac{\sum_{m=1}^M (\mathbf{W}^{(j)} \mathbf{x}_m - \mu_B)^2}{M} - \sigma^2 \right)^2 \right] \\
 &= \frac{1}{2\sigma\sqrt{M}} \left(\sum_{m=1}^M ((\mathbf{W}^{(j)} \mathbf{x}_m - \mu)^2 - \sigma^2) - \sum_{m=1}^M (\mu_B - \mu)^2 \right) + \\
 &\quad \mathcal{O} \left[\sqrt{M} \left(\frac{\sum_{m=1}^M (\mathbf{W}^{(j)} \mathbf{x}_m - \mu_B)^2}{M} - \sigma^2 \right)^2 \right] \\
 &= \frac{1}{2\sigma\sqrt{M}} \sum_{m=1}^M ((\mathbf{W}^{(j)} \mathbf{x}_m - \mu)^2 - \sigma^2) \\
 &\quad - \frac{1}{2\sigma\sqrt{M}} \sum_{m=1}^M (\mu_B - \mu)^2 \\
 &\quad + \mathcal{O} \left[\sqrt{M} \left(\frac{\sum_{m=1}^M (\mathbf{W}^{(j)} \mathbf{x}_m - \mu_B)^2}{M} - \sigma^2 \right)^2 \right] \\
 &= \underbrace{\frac{1}{2\sigma\sqrt{M}} \sum_{m=1}^M ((\mathbf{W}^{(j)} \mathbf{x}_m - \mu)^2 - \sigma^2)}_{\text{term A}} \\
 &\quad - \underbrace{\frac{\sqrt{M}}{2\sigma} (\mu_B - \mu)^2}_{\text{term B}} \\
 &\quad + \underbrace{\mathcal{O} \left[\sqrt{M} \left(\frac{\sum_{m=1}^M (\mathbf{W}^{(j)} \mathbf{x}_m - \mu_B)^2}{M} - \sigma^2 \right)^2 \right]}_{\text{term C}}
 \end{aligned}$$

We go through each term in turn

Term A

We have

$$\text{Term A} = \frac{1}{2\sigma\sqrt{M}} \sum_{m=1}^M ((\mathbf{W}^{(j)} \mathbf{x}_m - \mu)^2 - \sigma^2)$$

where $\sum_{m=1}^M (\mathbf{W}^{(j)} \mathbf{x}_m - \mu)^2$ is the sum of M RVs $(\mathbf{W}^{(j)} \mathbf{x}_m - \mu)^2$. Note that since $E[\mathbf{W}^{(j)} \mathbf{x}_m] = \mu$ it holds that $E[(\mathbf{W}^{(j)} \mathbf{x}_m - \mu)^2] = \sigma^2$. Since $(\mathbf{W}^{(j)} \mathbf{x}_m - \mu)^2$ is sampled approximately iid (by assumptions above), for large enough M by CLT it holds approximately that

$$\sum_{m=1}^M (\mathbf{W}^{(j)} \mathbf{x}_m - \mu)^2 \sim \mathcal{N}(M\sigma^2, M\text{Var}((\mathbf{W}^{(j)} \mathbf{x}_m - \mu)^2))$$

where

$$\begin{aligned}
 \text{Var}((\mathbf{W}^{(j)} \mathbf{x}_m - \mu)^2) &= E[(\mathbf{W}^{(j)} \mathbf{x}_m - \mu)^{2*2}] - E[(\mathbf{W}^{(j)} \mathbf{x}_m - \mu)^2]^2 \\
 &= E[(\mathbf{W}^{(j)} \mathbf{x}_m - \mu)^4] - \sigma^4
 \end{aligned}$$

Then

$$\sum_{m=1}^M ((\mathbf{W}^{(j)} \mathbf{x}_m - \mu)^2 - \sigma^2) \sim \mathcal{N}(0, M * E[(\mathbf{W}^{(j)} \mathbf{x}_m - \mu)^4] - M\sigma^4)$$

so

$$\text{Term A} \sim \mathcal{N}\left(0, \frac{E[(\mathbf{W}^{(j)} \mathbf{x}_m - \mu)^4] - \sigma^4}{4\sigma^2}\right)$$

Term B

We have

$$\text{Term B} = \frac{\sqrt{M}}{2\sigma}(\mu_B - \mu)^2 = \frac{1}{2\sigma}\sqrt{M}(\mu_B - \mu)(\mu_B - \mu)$$

Consider $(\mu_B - \mu)$. As $\mu_B \xrightarrow{p} \mu$ when $M \rightarrow \infty$ we have $\mu_B - \mu \xrightarrow{p} 0$. We also have

$$\sqrt{M}(\mu_B - \mu) = \frac{\sum_{m=1}^M \mathbf{W}^{(j)} \mathbf{x}_m}{\sqrt{M}} - \sqrt{M}\mu$$

which by CLT is approximately Gaussian for large M . We can then make use of the Cramer-Slutsky Theorem, which states that if $(X_n)_{n \geq 1}$ and $(Y_n)_{n \geq 1}$ are two sequences such that $X_n \xrightarrow{d} X$ and $Y_n \xrightarrow{p} a$ as $n \rightarrow \infty$ where a is a constant, then as $n \rightarrow \infty$, it holds that $X_n * Y_n \xrightarrow{d} X * a$. Thus, Term B is approximately 0 for large M .

Term C

We have

$$\text{Term C} = \mathcal{O}\left[\sqrt{M}\left(\frac{\sum_{m=1}^M (\mathbf{W}^{(j)} \mathbf{x}_m - \mu_B)^2}{M} - \sigma^2\right)^2\right]$$

Since $E[(\mathbf{W}^{(j)} \mathbf{x}_m - \mu)^2] = \sigma^2$ we can make the same use of Cramer-Slutsky as for *Term B*, such that Term C is approximately 0 for large M .

Finalizing the distribution

We have approximately

$$\sqrt{M}(\sigma_B - \sigma) \sim \mathcal{N}\left(0, \frac{E[(\mathbf{W}^{(j)} \mathbf{x}_m - \mu)^4] - \sigma^4}{4\sigma^2}\right)$$

so

$$\sigma_B \sim \mathcal{N}\left(\sigma, \frac{E[(\mathbf{W}^{(j)} \mathbf{x}_m - \mu)^4] - \sigma^4}{4\sigma^2 M}\right)$$

1.4. predictive distribution properties

This section provides derivations of properties of the predictive distribution $p^*(\mathbf{y}|\mathbf{x}, \mathbf{D})$ in section 3.4, following (Gal, 2016). We first find the approximate predictive mean and variance for the approximate predictive distribution, then show how to estimate the predictive log likelihood, a measure of uncertainty quality used in the evaluation.

Predictive mean Assuming Gaussian iid noise defined by model precision τ , i.e. $f_{\omega}(\mathbf{x}, \mathbf{y}) = p(\mathbf{y}|f_{\omega}(\mathbf{x})) = \mathcal{N}(\mathbf{y}; f_{\omega}(\mathbf{x}), \tau^{-1}\mathbf{I})$:

$$\begin{aligned} \mathbb{E}_{p^*}[\mathbf{y}] &= \int \mathbf{y} p^*(\mathbf{y}|\mathbf{x}, \mathbf{D}) d\mathbf{y} \\ &= \int_{\mathbf{y}} \mathbf{y} \left(\int_{\omega} f_{\omega}(\mathbf{x}, \mathbf{y}) q_{\theta}(\omega) d\omega \right) d\mathbf{y} \\ &= \int_{\mathbf{y}} \mathbf{y} \left(\int_{\omega} \mathcal{N}(\mathbf{y}; f_{\omega}(\mathbf{x}), \tau^{-1}\mathbf{I}) q_{\theta}(\omega) d\omega \right) d\mathbf{y} \\ &= \int_{\omega} \left(\int_{\mathbf{y}} \mathbf{y} \mathcal{N}(\mathbf{y}; f_{\omega}(\mathbf{x}), \tau^{-1}\mathbf{I}) d\mathbf{y} \right) q_{\theta}(\omega) d\omega \\ &= \int_{\omega} f_{\omega}(\mathbf{x}) q_{\theta}(\omega) d\omega \\ &\approx \frac{1}{T} \sum_{i=1}^T f_{\hat{\omega}_i}(\mathbf{x}) \end{aligned}$$

where we take the MC Integral with T samples of ω for the approximation in the final step.

Predictive variance Our goal is to estimate:

$$\text{Cov}_{p^*}[\mathbf{y}] = \mathbb{E}_{p^*}[\mathbf{y}^\top \mathbf{y}] - \mathbb{E}_{p^*}[\mathbf{y}]^\top \mathbb{E}_{p^*}[\mathbf{y}]$$

We find that:

$$\begin{aligned} \mathbb{E}_{p^*}[\mathbf{y}^\top \mathbf{y}] &= \int_{\mathbf{y}} \mathbf{y}^\top \mathbf{y} p^*(\mathbf{y} | \mathbf{x}, \mathbf{D}) d\mathbf{y} \\ &= \int_{\mathbf{y}} \mathbf{y}^\top \mathbf{y} \left(\int_{\omega} f_{\omega}(\mathbf{x}, \mathbf{y}) q_{\theta}(\omega) d\omega \right) d\mathbf{y} \\ &= \int_{\omega} \left(\int_{\mathbf{y}} \mathbf{y}^\top \mathbf{y} f_{\omega}(\mathbf{x}, \mathbf{y}) d\mathbf{y} \right) q_{\theta}(\omega) d\omega \\ &= \int_{\omega} \left(\text{Cov}_{f_{\omega}(\mathbf{x}, \mathbf{y})}(\mathbf{y}) + \mathbb{E}_{f_{\omega}(\mathbf{x}, \mathbf{y})}[\mathbf{y}]^\top \mathbb{E}_{f_{\omega}(\mathbf{x}, \mathbf{y})}[\mathbf{y}] \right) q_{\theta}(\omega) d\omega \\ &= \int_{\omega} \left(\tau^{-1} \mathbf{I} + f_{\omega}(\mathbf{x})^\top f_{\omega}(\mathbf{x}) \right) q_{\theta}(\omega) d\omega \\ &= \tau^{-1} \mathbf{I} + E_{q_{\theta}(\omega)}[f_{\omega}(\mathbf{x})^\top f_{\omega}(\mathbf{x})] \\ &\approx \tau^{-1} \mathbf{I} + \frac{1}{T} \sum_{i=1}^T f_{\hat{\omega}_i}(\mathbf{x})^\top f_{\hat{\omega}_i}(\mathbf{x}) \end{aligned}$$

where we use MC integration with T samples for the final step. The predictive covariance matrix is given by:

$$\text{Cov}_{p^*}[\mathbf{y}] \approx \tau^{-1} \mathbf{I} + \frac{1}{T} \sum_{i=1}^T f_{\hat{\omega}_i}(\mathbf{x})^\top f_{\hat{\omega}_i}(\mathbf{x}) - \mathbb{E}_{p^*}[\mathbf{y}]^\top \mathbb{E}_{p^*}[\mathbf{y}]$$

which is the sum of the variance from observation noise and the sample covariance from T stochastic forward passes through the network.

The form of p^* can be approximated by a Gaussian for each output dimension (for regression). We assume bounded domains for each input dimension, wide layers throughout the network, and a uni-modal distribution of weights centered at 0. By the Liapounov CLT condition, the first layer then receives approximately Gaussian inputs (a proof can be found in (Lehmann, 1999)). Having sampled μ_B^u and σ_B^u from a mini-batch, each BN unit's output is bounded. CLT thereby continues to hold for deeper layers, including $f_{\omega}(\mathbf{x}) = \mathbf{W}^L \mathbf{x}^L$. A similar motivation for a Gaussian approximation of Dropout has been presented by (Wang & Manning, 2013).

Predictive Log Likelihood We use the Predictive Log Likelihood (PLL) as a measure to estimate the model's uncertainty quality. For a certain test point $(\mathbf{y}_i, \mathbf{x}_i)$, the PLL definition and approximation can be expressed as:

$$\begin{aligned} \text{PLL}(f_{\omega}(\mathbf{x}), (\mathbf{y}_i, \mathbf{x}_i)) &= \log p(\mathbf{y}_i | f_{\omega}(\mathbf{x}_i)) \\ &= \log \int f_{\omega}(\mathbf{x}_i, \mathbf{y}_i) p(\omega | \mathbf{D}) d\omega \\ &\approx \log \int f_{\omega}(\mathbf{x}_i, \mathbf{y}_i) q_{\theta}(\omega) d\omega \\ &\approx \log \sum_{j=1}^T p(\mathbf{y}_i | f_{\hat{\omega}_j}(\mathbf{x}_i)) \end{aligned}$$

where $\hat{\omega}_j$ represents a sampled set of stochastic parameters from the approximate posterior distribution $q_{\theta}(\omega)$ and we take a MC integration with T samples. For regression, due to the iid Gaussian noise, we can further develop the derivation into

the form we use when sampling:

$$\begin{aligned}
 \text{PLL}(f_{\omega}(\mathbf{x}), (\mathbf{y}_i, \mathbf{x}_i)) &= \log \sum_{i=1}^T \mathcal{N}(\mathbf{y}_i | f_{\omega_j}(\mathbf{x}_i), \tau^{-1} \mathbf{I}) \\
 &= \text{logsumexp}_{j=1, \dots, T} \left(-\frac{1}{2} \|\mathbf{y}_i - f_{\omega_j}(\mathbf{x}_i)\|^2 \right) \\
 &\quad + \log T - \frac{1}{2} \log 2\pi + \frac{1}{2} \log \tau
 \end{aligned}$$

Note that PLL makes no assumption on the form of the approximate predictive distribution. The measure is based on repeated sampling $\hat{\omega}_j$ from $q_{\theta}(\omega)$, which may be highly multimodal (see section 3.4).

1.5. Prior

We assume training by SGD with mini-batch size M , L2-regularization on weights and Fully Connected layers. With $\theta_k \in \theta$, equivalence between the objectives of Eq. (1) and (2) then requires:

$$\begin{aligned}
 \frac{\partial}{\partial \theta_k} \text{KL}(q_{\theta}(\omega) || p(\omega)) &= N\tau \frac{\partial}{\partial \theta_k} \Omega(\theta) \\
 &= N\tau \frac{\partial}{\partial \theta_k} \sum_{l=1}^L \lambda_l \|\mathbf{W}^l\|^2
 \end{aligned} \tag{5}$$

To proceed with the LHS of Eq. (5) we first need to find the approximate posterior $q_{\theta}(\omega)$ that batch normalization induces. As shown in Appendix 1.3, with some weak assumptions and approximations the Central Limit Theorem (CLT) yields Gaussian distributions of the stochastic variables $\mu_{\mathbf{B}}^u, \sigma_{\mathbf{B}}^u$, for large enough M :

$$\begin{aligned}
 \mu_{\mathbf{B}}^u &\lesssim \mathcal{N}(\mu^u, \frac{(\sigma^u)^2}{M}), \\
 \sigma_{\mathbf{B}}^u &\lesssim \mathcal{N}(\sigma^u, \frac{\mathbb{E}[(h^u - \mu^u)^4] - (\sigma^u)^4}{4(\sigma^u)^2 M})
 \end{aligned} \tag{6}$$

where μ^u and σ^u are the *population-level* moments (i.e. moments over \mathbf{D}), and h^u is the BN unit's input. We use i as an index of the set of stochastic variables, i.e. $\omega_i \in \{\mu_{\mathbf{B}}^{1:L}, \sigma_{\mathbf{B}}^{1:L}\}$, and denote by ω_i^l the stochastic variables in a certain layer, $\omega_i^l \in \{\mu_{\mathbf{B}}^l, \sigma_{\mathbf{B}}^l\}$. We assume $q_{\theta}(\omega)$ and $p(\omega)$ factorize over all individual ω_i , i.e. independence between all stochastic variables.¹³ As shown in Eq. (3) in Appendix 1.2, the factorized distributions yield:

$$\text{KL}(q_{\theta}(\omega) || p(\omega)) = \sum_i \text{KL}(q_{\theta}(\omega_i) || p(\omega_i))$$

Note that each BN unit produces two $\text{KL}(q_{\theta}(\omega_i) || p(\omega_i))$ terms: one for $\omega_i = \mu_{\mathbf{B}}^u$ and one for $\omega_i = \sigma_{\mathbf{B}}^u$.

We assume a Gaussian prior $p(\omega_i) = \mathcal{N}(\mu_p, \sigma_p^2)$ and, for consistency, use the notation $q_{\theta}(\omega_i) = \mathcal{N}(\mu_q, \sigma_q^2)$. As shown in Eq. (4) in Appendix 1.2:

$$\text{KL}(q_{\theta}(\omega_i) || p(\omega_i)) = \ln \frac{\sigma_p}{\sigma_q} + \frac{\sigma_q^2 + (\mu_q - \mu_p)^2}{2\sigma_p^2} - \frac{1}{2}$$

Then, letting $(\cdot)'$ denote $\frac{\partial}{\partial \theta_k}(\cdot)$:

$$\begin{aligned}
 \frac{\partial}{\partial \theta_k} \text{KL}(q_{\theta}(\omega_i) || p(\omega_i)) &= \frac{2\sigma_q \sigma_p \sigma'_q - \sigma'_p (2\sigma_q^2 - (\mu_q - \mu_p)^2)}{\sigma_p^3} + \frac{(\mu_q - \mu_p)(\mu'_q - \mu'_p)}{\sigma_p^2} \\
 &= \frac{2\sigma_p \sigma_q \sigma'_q}{\sigma_p^3} + \frac{(\mu_q - \mu_p)\mu'_q}{\sigma_p^2}
 \end{aligned} \tag{7}$$

¹³The empirical distributions have been numerically checked to be linearly independent and the joint distribution is close to a bi-variate Gaussian.

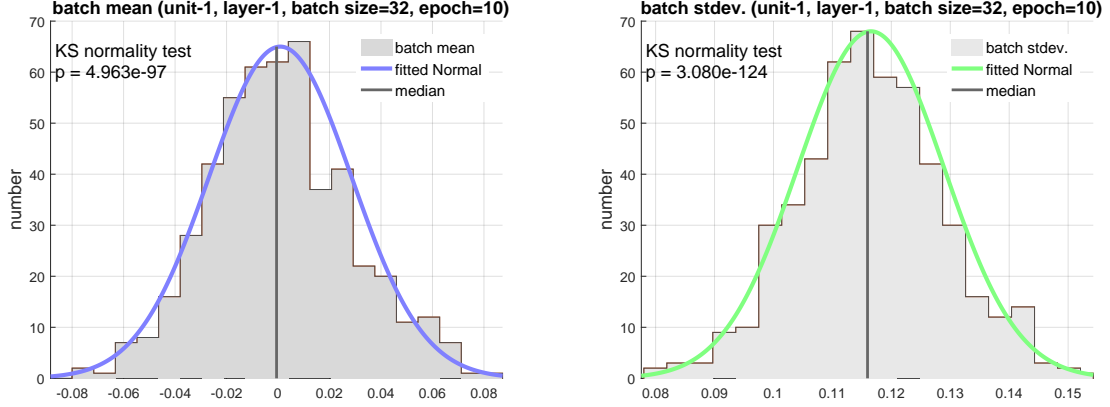


Figure 3. Batch statistics used to train the network are normal. A one-sample Kolmogorov-Smirnov test checks that μ_B and σ_B come from a standard normal distribution. More examples are available in Appendix 1.8.

where the last step makes use of the fact that $\mu'_p = 0$ and $\sigma'_p = 0$ (as $p(\omega_i)$ cannot depend on θ_k , which changes during training).

We assume that only parameters preceding a BN unit in the same layer affects the unit's stochastic parameters, such that the stochastic variables in the j :th BN unit are only affected by weights in $\theta_k \in \mathbf{W}^{l,(j)}$. Let the vector of average inputs over \mathbf{D} from the preceding layers be denoted by \bar{x} . We denote a weight connecting the m :th input unit to the j :th BN unit by $\mathbf{W}^{(j,m)}$. For such weights, we need to derive μ'_q and σ'_q , for both $\omega_i = \mu_B^u$ and $\omega_i = \sigma_B^u$. Starting with $\omega_i = \mu_B^u$:

$$\begin{aligned}\mu'_q &= \frac{\partial}{\partial \mathbf{W}^{(j,m)}} \frac{\sum_{\mathbf{x} \in \mathbf{D}} \mathbf{W}^{(j)} \mathbf{x}}{N} = \bar{x}^{(m)} \\ \sigma'_q &= \frac{\partial}{\partial \mathbf{W}^{(j,m)}} \left[\frac{\sum_{\mathbf{x} \in \mathbf{D}} (\mathbf{W}^{(j)} \mathbf{x} - \mu_q)^2}{NM} \right]^{\frac{1}{2}} \\ &= \frac{1}{2} \left[\frac{\sum_{\mathbf{x} \in \mathbf{D}} (\mathbf{W}^{(j)} \mathbf{x} - \mu_q)^2}{NM} \right]^{-\frac{1}{2}} \frac{\sum_{\mathbf{x} \in \mathbf{D}} 2(\mathbf{W}^{(j)} \mathbf{x} - \mu_q)(\mathbf{x}^{(m)} - \bar{x}^{(m)})}{NM} = 0\end{aligned}$$

Using the result that $\sigma'_q = 0$, one can easily find for $\omega_i = \sigma_B^u$ that $\mu'_q = 0$ and $\sigma'_q = 0$, nullifying Eq. (7). We need only consider the partial derivatives of the KL divergence terms where $\omega_i = \mu_B^u$. If we let $\mu_p = 0$, Eq. (7) reduces to:

$$\frac{\partial}{\partial \mathbf{W}^{(j,m)}} \text{KL}(q_{\theta}(\omega_i) || p(\omega_i)) = \frac{\mu_q \bar{x}^{(m)}}{\sigma_p^2} = \frac{\bar{x}^{(m)} \mathbf{W}^{(j)} \bar{x}}{\sigma_p^2}$$

for each BN unit and connecting weights from the previous layer, $\mathbf{W}^{(j,m)}$. Taking partial derivatives for all $\text{KL}(q_{\theta}(\omega_i) || p(\omega_i))$ components in the layer:

$$\sum_{\omega_i^l} \sum_j \sum_m \frac{\partial}{\partial \mathbf{W}^{(j,m)}} \text{KL}(q_{\theta}(\omega_i) || p(\omega_i)) = \sum_m [\bar{x}^{(m)}] * \sum_j \sum_m \frac{\mathbf{W}^{(j,m)} \bar{x}^{(m)}}{\sigma_p^2} \quad (8)$$

We consider ReLU activations, such that for large N , $\bar{x}^{(m)} > 0 \quad \forall m$. Note that this does not hold for the first layer (which is possibly normalized), but the effect of including these weights in the L2-regularization would be smaller the deeper the network. We assume most outputs from previous layer's BN units remain normalized through the scale and shift transformation, such that we can approximate $\bar{x}^{(m)}$ by the average of all input units over test data, x in Eq. (8). With J_{l-1} units in the input layer, setting $\sigma_p^2 = \frac{J_{l-1} x^2}{2N\lambda_l}$, such that $p(\mu_B^u) = \mathcal{N}(0, \frac{J_{l-1} x^2}{2N\tau\lambda_l})$ would then reconcile Eq. (5), for any Gaussian $p(\sigma_B^u)$.

1.6. Extended experimental results

Below, we provide extended results measuring uncertainty quality. In Tables 3 and 4, we provide tables showing the mean CRPS and PLL values for MCBN and MCDO. These results indicate that MCBN performs on par or better than MCDO

across several datasets. In Table 5 we provide the raw PLL and CRPS results for MCBN and MCDO. In Table 6 we provide RMSE results of the MCBN and MCDO networks in comparison with non-stochastic BN and DO networks. These results indicate that the procedure of multiple forward passes in MCBN and MCDO show slight improvements in the accuracy of the network.

In Figure 4 and Figure 5, we provide a full set of our uncertainty quality visualization plots, where errors in predictions are sorted by estimated uncertainty. The shaded areas show the model uncertainty and gray dots show absolute prediction errors on the test set. A gray line depicts a running mean of the errors. The dashed line indicates the optimized constant uncertainty. In these plots, we can see a correlation between estimated uncertainty (shaded area) and mean error (gray). This trend indicates that the model uncertainty estimates can recognize samples with larger (or smaller) potential for predictive errors.

Table 3. CRPS measured on eight datasets over 5 random 80-20 splits of the data with 5 different random seeds each split. Mean values for MCBN, MCDO and MNF are reported along with standard error. A significance test was performed to check if CRPS significantly exceeds the baseline. The p -value from a one sample t-test is reported.

Dataset	CRPS					
	MCBN	p -value	MCDO	p -value	MNF	p -value
Boston Housing	8.50 \pm 0.86	6.39E-10	3.06 \pm 0.33	1.64E-09	5.88 \pm 1.09	2.01E-05
Concrete	3.91 \pm 0.25	4.53E-14	0.93 \pm 0.41	3.13E-02	3.13 \pm 0.81	6.43E-04
Energy Efficiency	5.75 \pm 0.52	6.71E-11	1.37 \pm 0.89	1.38E-01	1.10 \pm 2.63	6.45E-01
Kinematics 8nm	2.85 \pm 0.18	2.33E-14	1.82 \pm 0.14	1.64E-12	0.52 \pm 0.26	7.15E-02
Power Plant	0.24 \pm 0.05	2.32E-04	-0.44 \pm 0.05	2.17E-08	-0.89 \pm 0.15	3.36E-06
Protein	2.66 \pm 0.10	2.77E-12	0.99 \pm 0.08	2.34E-12	0.57 \pm 0.03	8.56E-16
Wine Quality (Red)	0.26 \pm 0.07	1.26E-03	2.00 \pm 0.21	1.83E-09	0.93 \pm 0.12	6.19E-08
Yacht Hydrodynamics	-56.39 \pm 14.27	5.94E-04	21.42 \pm 2.99	2.16E-07	24.92 \pm 3.77	9.62E-06

Table 4. PLL measured on eight datasets over 5 random 80-20 splits of the data with 5 different random seeds each split. Mean values for MCBN, MCDO and MNF are reported along with standard error. A significance test was performed to check if PLL significantly exceeds the baseline. The p -value from a one sample t-test is reported.

Dataset	PLL					
	MCBN	p -value	MCDO	p -value	MNF	p -value
Boston Housing	10.49 \pm 1.35	5.41E-08	5.51 \pm 1.05	2.20E-05	1.76 \pm 1.12	1.70E-01
Concrete	-36.36 \pm 12.12	6.19E-03	10.92 \pm 1.78	2.34E-06	-2.16 \pm 4.19	6.79E-01
Energy Efficiency	10.89 \pm 1.16	1.79E-09	-14.28 \pm 5.15	1.06E-02	-33.88 \pm 29.57	2.70E-01
Kinematics 8nm	1.68 \pm 0.37	1.29E-04	-0.26 \pm 0.18	1.53E-01	0.42 \pm 0.43	2.70E-01
Power Plant	0.33 \pm 0.14	2.72E-02	3.52 \pm 0.23	1.12E-13	-0.86 \pm 0.15	7.33E-06
Protein	2.56 \pm 0.23	4.28E-11	6.23 \pm 0.19	2.57E-21	0.52 \pm 0.07	1.81E-07
Wine Quality (Red)	0.19 \pm 0.09	3.72E-02	2.91 \pm 0.35	1.84E-08	0.83 \pm 0.16	2.27E-05
Yacht Hydrodynamics	45.58 \pm 5.18	5.67E-09	-41.54 \pm 31.37	1.97E-01	46.19 \pm 4.45	2.47E-07

1.7. Uncertainty in image segmentation

We applied MCBN to an image segmentation task using Bayesian SegNet with the main CamVid and PASCAL-VOC models in (Kendall et al., 2015). Here, we provide more image from Pascal VOC dataset in Figure 6.

1.8. Batch normalization statistics

In Figure 7 and Figure 8, we provide statistics on the batch normalization parameters used for training. The plots show the distribution of BN mean and BN variance over different mini-batches of an actual training of Yacht dataset for one unit in the first hidden layer and the second hidden layer. Data is provided for different epochs and for different batch sizes.

Table 5. CRPS and PLL measured on eight datasets over 5 random 80-20 splits of the data with 5 different random seeds each split. Mean values and standard errors are reported for MCBN, MCDO and MNF.

Dataset	CRPS			PLL		
	MCBN	MCDO	MNF	MCBN	MCDO	MNF
Boston Housing	1.45±0.02	1.41±0.02	1.57±0.02	-2.38±0.02	-2.35±0.02	-2.51±0.06
Concrete	2.40±0.04	2.42±0.04	3.61±0.02	-3.45±0.11	-2.94±0.02	-3.35±0.04
Energy Efficiency	0.33±0.01	0.26±0.00	1.33±0.04	-0.94±0.04	-0.80±0.04	-3.18±0.07
Kinematics 8nm	0.04±0.00	0.04±0.00	0.05±0.00	1.21±0.01	1.24±0.00	1.04±0.00
Power Plant	2.00±0.01	2.00±0.01	2.31±0.01	-2.75±0.00	-2.72±0.01	-2.86±0.01
Protein	1.95±0.01	1.95±0.00	2.25±0.01	-2.73±0.00	-2.70±0.00	-2.83±0.01
Wine Quality (Red)	0.34±0.00	0.33±0.00	0.34±0.00	-0.95±0.01	-0.89±0.01	-0.93±0.00
Yacht Hydrodynamics	0.68±0.02	0.32±0.01	0.94±0.01	-1.39±0.03	-2.57±0.69	-1.96±0.05

Table 6. RMSE measured on eight datasets over 5 random 80-20 splits of the data with 5 different random seeds each split. Mean values and standard errors are reported for MCBN, MCDO and MNF as well as conventional non-Bayesian models BN and DO.

Dataset	RMSE				
	MCBN	BN	MCDO	DO	MNF
Boston Housing	2.75±0.05	2.77±0.05	2.65±0.05	2.69±0.05	2.98±0.06
Concrete	4.78±0.09	4.89±0.08	4.80±0.10	4.99±0.10	6.57±0.04
Energy Efficiency	0.59±0.02	0.57±0.01	0.47±0.01	0.49±0.01	2.38±0.07
Kinematics 8nm	0.07±0.00	0.07±0.00	0.07±0.00	0.07±0.00	0.09±0.00
Power Plant	3.74±0.01	3.74±0.01	3.74±0.02	3.72±0.02	4.19±0.01
Protein	3.66±0.01	3.69±0.01	3.66±0.01	3.68±0.01	4.10±0.01
Wine Quality (Red)	0.62±0.00	0.62±0.00	0.60±0.00	0.61±0.00	0.61±0.00
Yacht Hydrodynamics	1.23±0.05	1.28±0.06	0.75±0.03	0.72±0.04	2.13±0.05

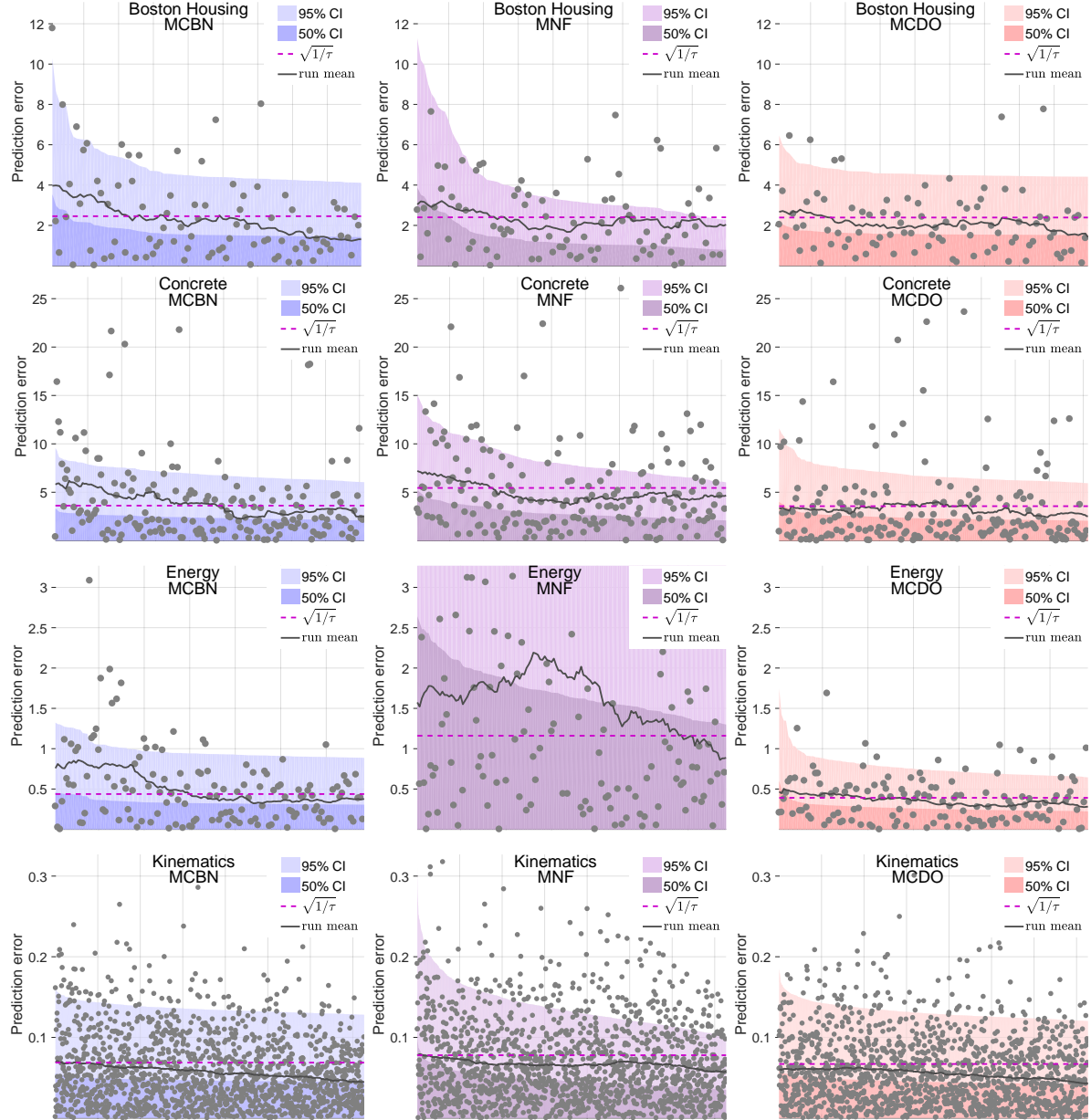


Figure 4. Errors in predictions (gray dots) sorted by estimated uncertainty on select datasets. The shaded areas show model uncertainty (light area 95% CI, dark area 50% CI). Gray dots show absolute prediction errors on the test set, and the gray line depicts a running mean of the errors. The dashed line indicates the optimized constant uncertainty. A correlation between estimated uncertainty (shaded area) and mean error (gray) indicates the uncertainty estimates are meaningful for estimating errors.

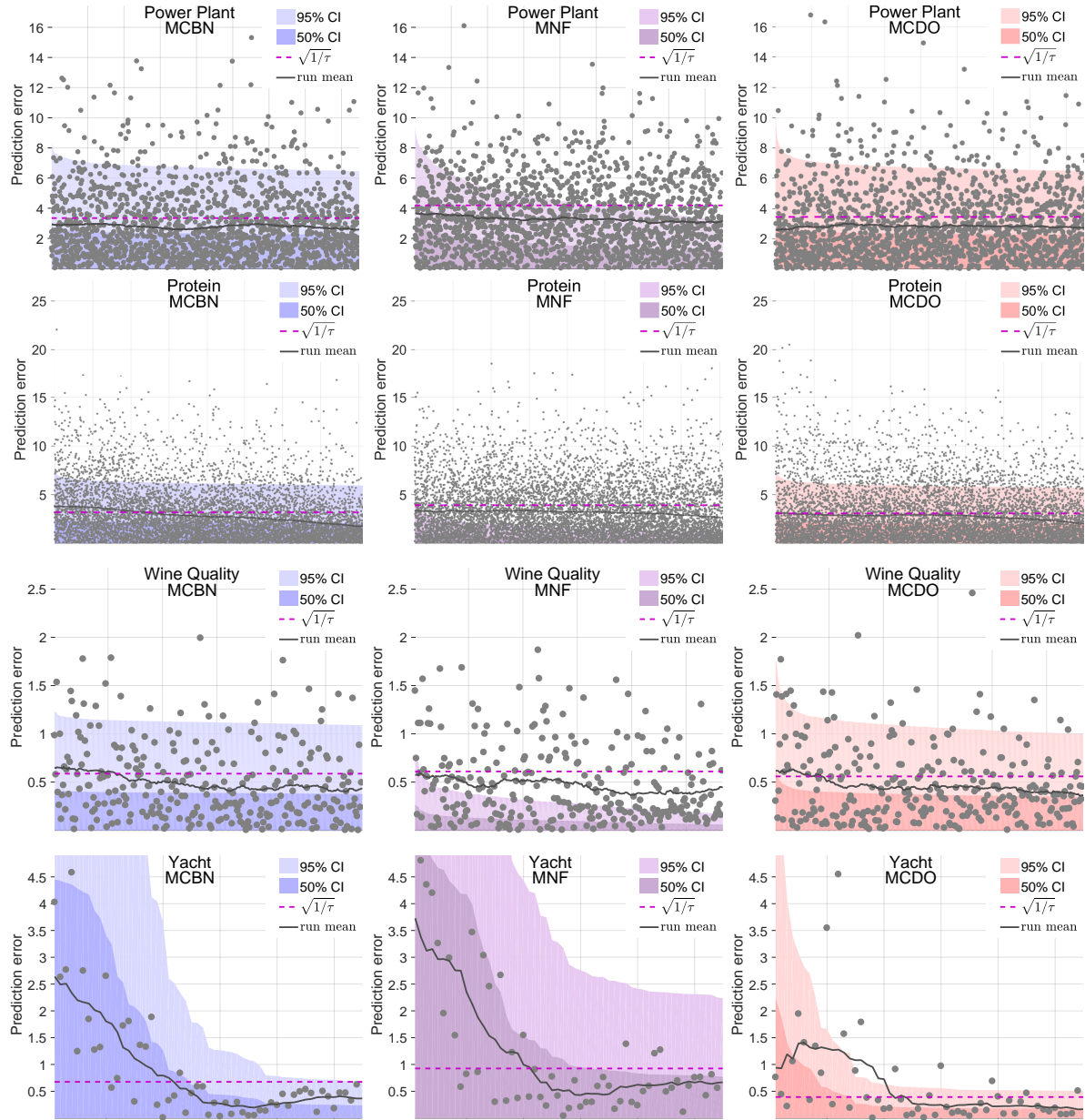


Figure 5. Errors in predictions (gray dots) sorted by estimated uncertainty on select datasets. The shaded areas show model uncertainty (light area 95% CI, dark area 50% CI). Gray dots show absolute prediction errors on the test set, and the gray line depicts a running mean of the errors. The dashed line indicates the optimized constant uncertainty. A correlation between estimated uncertainty (shaded area) and mean error (gray) indicates the uncertainty estimates are meaningful for estimating errors.

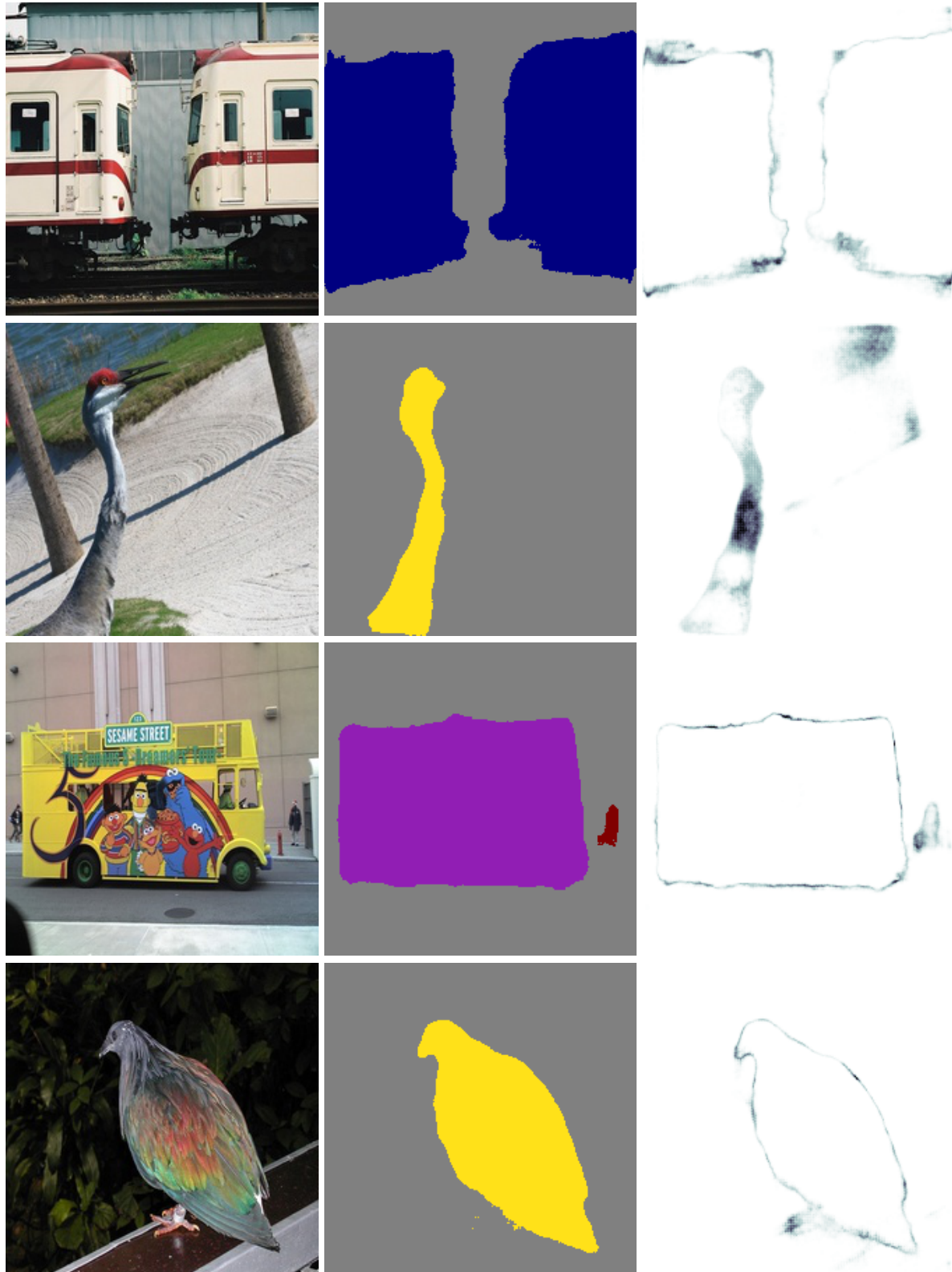


Figure 6. Uncertainty in image segmentation. Results applying MCBN to Bayesian SegNet (Kendall et al., 2015) on images from PASCAL-VOC (right). Left: original. Middle: the Bayesian estimated segmentation. Right: estimated uncertainty using MCBN for all classes. Mini-batches of size 36 were used for PASCAL-VOC on images of size 224x224. 20 inferences were conducted to estimate the mean and variance of MCBN.

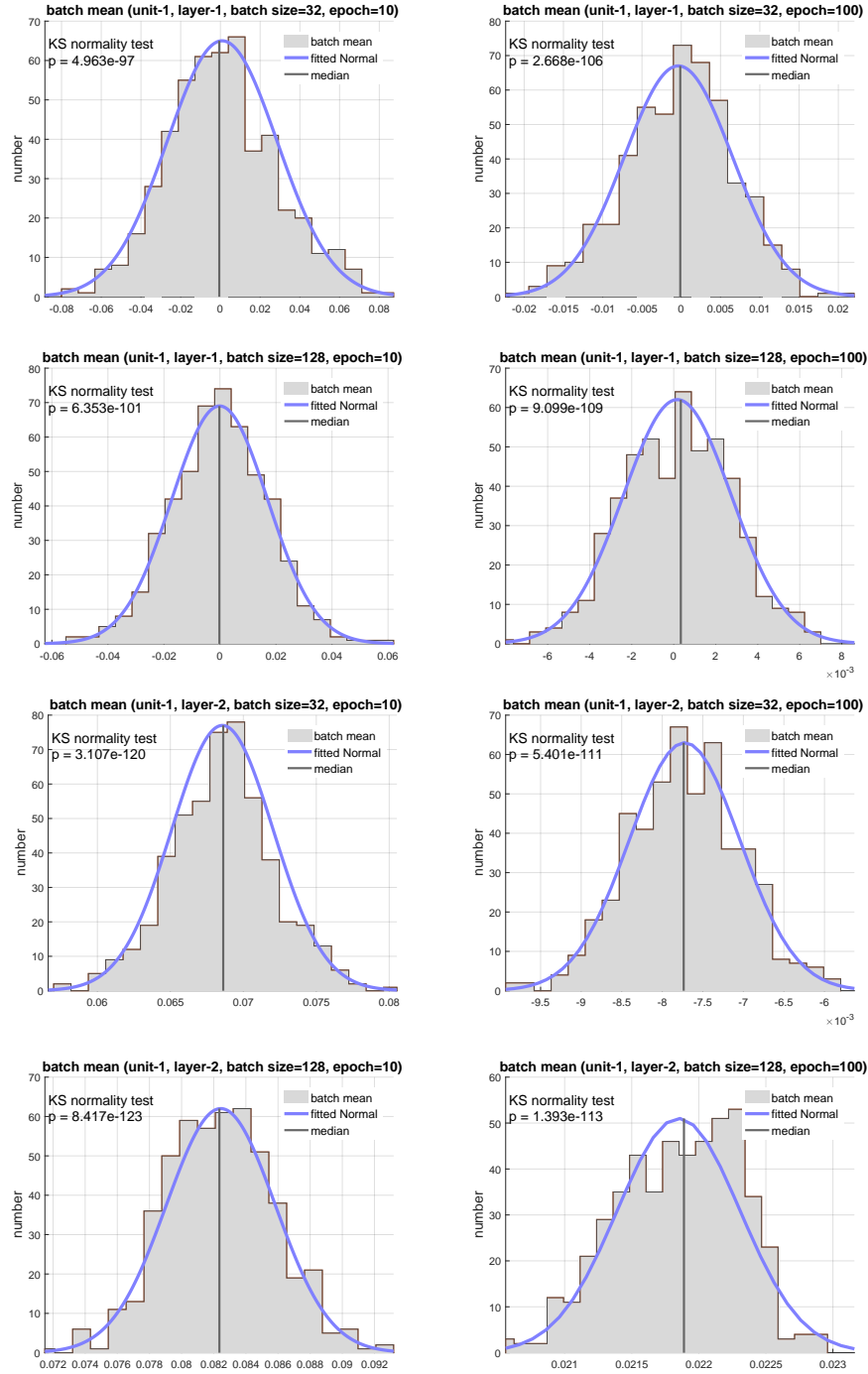


Figure 7. The distribution of means of mini-batches during training of one of our datasets. The distribution closely follows our analytically approximated Gaussian distribution. The data is collected for one unit of each layer and is provided for different epochs and for different batch sizes.

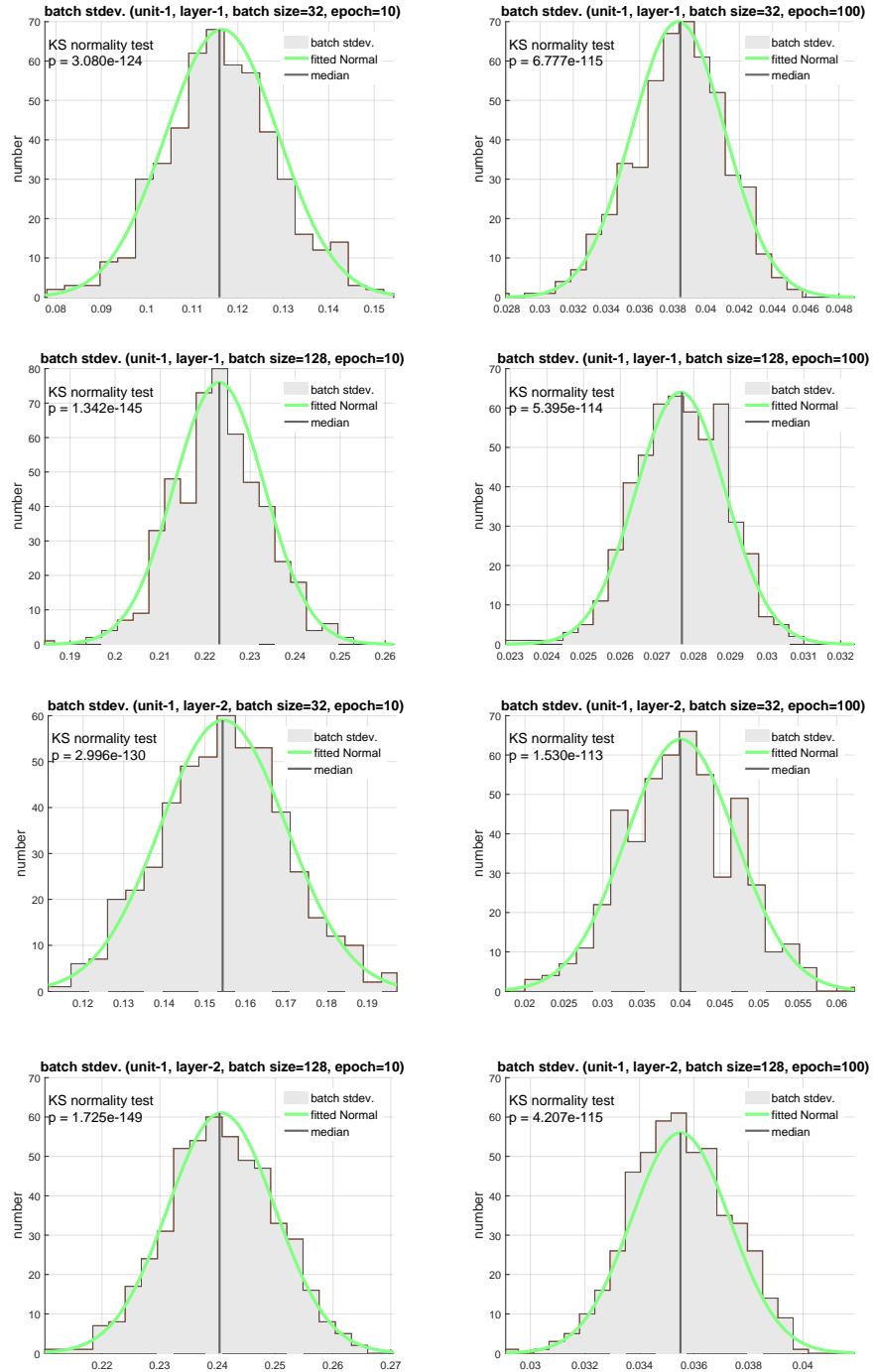


Figure 8. The distribution of standard deviation of mini-batches during training of one of our datasets. The distribution closely follows our analytically approximated Gaussian distribution. The data is collected for one unit of each layer and is provided for different epochs and for different batch sizes.